

Paclitaxel enhances the innate immunity by promoting NLRP3 inflammasome activation in macrophages

Qiong-zhen Zeng¹, Fan Yang¹, Chen-Guang Li¹, Li-hui Xu¹, Xian-Hui He¹, Feng-yi Mai¹,
Chen-ying Zeng¹, Cheng-cheng Zhang¹, Qing-bing Zha^{1*}, Dong-Yun Ouyang^{1*}

¹Jinan University, China

Submitted to Journal:
Frontiers in Immunology

Specialty Section:
Molecular Innate Immunity

ISSN:
1664-3224

Article type:
Original Research Article

Received on:
24 Oct 2018

Accepted on:
11 Jan 2019

Provisional PDF published on:
11 Jan 2019

Frontiers website link:
www.frontiersin.org

Citation:

Zeng Q, Yang F, Li C, Xu L, He X, Mai F, Zeng C, Zhang C, Zha Q and Ouyang D(2018) Paclitaxel enhances the innate immunity by promoting NLRP3 inflammasome activation in macrophages. *Front. Immunol.* 10:72. doi:10.3389/fimmu.2019.00072

Copyright statement:

© 2019 Zeng, Yang, Li, Xu, He, Mai, Zeng, Zhang, Zha and Ouyang. This is an open-access article distributed under the terms of the [Creative Commons Attribution License \(CC BY\)](https://creativecommons.org/licenses/by/4.0/). The use, distribution and reproduction in other forums is permitted, provided the original author(s) or licensor are credited and that the original publication in this journal is cited, in accordance with accepted academic practice. No use, distribution or reproduction is permitted which does not comply with these terms.

15 **ABSTRACT**

16 Microtubules play critical roles in regulating the activation of NLRP3
17 inflammasome and microtubule-destabilizing agents such as colchicine have been
18 shown to suppress the activation of this inflammasome. However, it remains largely
19 unknown whether paclitaxel, a microtubule-stabilizing agent being used in cancer
20 therapy, has any influences on NLRP3 inflammasome activation. Here we showed
21 that paclitaxel pre-treatment greatly enhanced ATP- or nigericin-induced NLRP3
22 inflammasome activation as indicated by increased release of cleaved caspase-1 and
23 mature IL-1 β , enhanced formation of ASC speck, and increased gasdermin D
24 cleavage and pyroptosis. Paclitaxel time- and dose-dependently induced α -tubulin
25 acetylation in LPS-primed murine and human macrophages and further increased
26 ATP- or nigericin-induced α -tubulin acetylation. Such increased α -tubulin acetylation
27 was significantly suppressed either by resveratrol or NAD⁺ (coenzyme required for
28 deacetylase activity of SIRT2), or by genetic knockdown of *MEC-17* (gene encoding
29 α -tubulin acetyltransferase 1). Concurrently, the paclitaxel-mediated enhancement of
30 NLRP3 inflammasome activation was significantly suppressed by resveratrol, NAD⁺,
31 or *MEC-17* knockdown, indicating the involvement of paclitaxel-induced α -tubulin
32 acetylation in the augmentation of NLRP3 inflammasome activation. Similar to
33 paclitaxel, epothilone B that is another microtubule-stabilizing agent also induced
34 α -tubulin acetylation and increased NLRP3 inflammasome activation in macrophages
35 in response to ATP treatment. Consistent with the *in vitro* results, intraperitoneal
36 administration of paclitaxel significantly increased serum IL-1 β levels, reduced
37 bacterial burden, dampened infiltration of inflammatory cells in the liver, and
38 improved animal survival in a mouse model of bacterial infection. Collectively, our
39 data indicate that paclitaxel potentiated NLRP3 inflammasome activation by inducing
40 α -tubulin acetylation and thereby conferred enhanced antibacterial innate responses,
41 suggesting its potential application against pathogenic infections beyond its use as a
42 chemotherapeutic agent.

43 **Key words:** paclitaxel, NLRP3 inflammasome, α -tubulin acetylation, MEC-17,

44 SIRT2

45

Provisional

46 INTRODUCTION

47 Paclitaxel is a first-line chemotherapeutic medicine. In clinic, it is used for the
48 treatment of a broad spectrum of cancers, including breast cancer, lung cancer, as well
49 as ovarian, cervical and pancreatic cancers (1-4). It is clinically used intravenously,
50 and its distribution throughout the body is rapid, with large volumes of distribution (5).
51 It has been known that paclitaxel is a microtubule-stabilizing agent. Mechanistically,
52 paclitaxel binds to the β -unit of microtubule (β -tubulin), thus stabilizing the α/β
53 polymer, and suppressing the organization capacity of centrosomes (5,6). In mitotic
54 cells, paclitaxel prevents the mitotic spindle from disassembly (7). Therefore, the
55 mitotic cells treated with paclitaxel cannot proceed into metaphase and are doomed to
56 apoptosis due to cell cycle arrest (8,9) and reduced mitochondrial membrane potential
57 (10). However, it has been demonstrated that paclitaxel affects microtubule dynamics
58 at concentrations much lower than those inhibiting mitosis and cell division (11).

59 NLPR3 [NOD-like receptor (NLR) family, pyrin containing domain 3] is a
60 critical cytosolic receptor that can sense bacterial, fungal and viral infections, as well
61 as other signal molecules such as extracellular ATP (released during bacterial
62 infection or tissue damage), nigericin (a microbial toxin derived from *Streptomyces*
63 *hygroscopicus*), and monosodium urate crystals (MSU, causative factor of gout) (12).
64 Full activation of NLRP3 inflammasome requires two inflammatory signals. The first
65 (priming signal) is provided by interaction of a microbe-associated molecular pattern
66 (MAMP) with its pattern recognition receptor (PRR), which induces activation of the
67 NF- κ B signaling pathway and expression of NLRP3, pro-interleukin (IL)-1 β and
68 pro-IL-18, and the second comes from various stimulators including damage
69 associated molecular patterns (DAMPs), such as extracellular ATP (13). Upon these
70 inflammatory stimulations, NLRP3 molecules recruit the adaptor protein ASC
71 (apoptosis-associated speck-like protein containing a CARD) to form a large platform
72 (i.e., NLRP3 inflammasome) for pro-caspase-1 binding, leading to its activation by
73 autocatalytic processing. The active caspase-1 in turn proteolytically cleaves
74 pro-IL-1 β and pro-IL-18 into mature IL-1 β and IL-18, which are subsequently

75 released to potentiate the innate immunity or inflammation (14). Concomitantly,
76 active caspase-1 also cleaves gasdermin D (GSDMD) to produce an N-terminal
77 fragment (GSDMD-NT), which forms pores on the plasma membrane and thereby
78 mediating programmed cell death named pyroptosis (15). Some studies have indicated
79 that cell membrane rupture and pyroptosis is required for the release of IL-1 β and
80 other inflammatory factors (16), suggesting that pyroptosis is an important process in
81 mediating inflammation.

82 Recently, published studies showed that microtubules have important roles in
83 regulating the assembly of NLRP3 inflammasome (17,18). It has been shown that
84 colchicine, a microtubule-destabilizing drug that binds to β -tubulin and inhibits
85 microtubule polymerization (19), suppresses NLRP3 inflammasome activation (17).
86 Owing to the effect of colchicine on suppressing MSU-induced NLRP3
87 inflammasome activation, thus dampening IL-1 β release and neutrophil recruitment
88 (20), it has long been used in clinic for the treatment of gout (21-23). Opposite to the
89 action mechanism of colchicine, paclitaxel stabilizes microtubule and mitotic spindle
90 by binding to β -tubulin (24). Although paclitaxel has been implicated in NLRP3
91 inflammasome activation (25), its action on the inflammasome activation and the
92 underlying mechanism are still incompletely understood. In this study, we revealed
93 that paclitaxel dose- and time-dependently enhanced α -tubulin acetylation in
94 lipopolysaccharide (LPS)-primed macrophages. Paclitaxel treatment greatly enhanced
95 NLRP3 inflammasome activation, as indicated by increased mature IL-1 β release,
96 ASC speck formation and pyroptosis, in LPS-primed macrophages in response to ATP
97 or nigericin stimulation. Inhibition of α -tubulin acetylation with resveratrol and NAD⁺,
98 two activators of deacetylase SIRT2, or knockdown of the α -tubulin acetyltransferase
99 MEC-17 expression attenuated paclitaxel-mediated augmentation of NLRP3
100 inflammasome activation. Moreover, intraperitoneal paclitaxel administration
101 improved the survival of mice against bacterial infection. Our results suggest that
102 paclitaxel enhanced the innate immune response against bacterial infection by
103 enhancing NLRP3 inflammasome activation through inducing α -tubulin acetylation.

104 MATERIALS AND METHODS

105 Reagents and antibodies

106 Paclitaxel (P106868) was purchased from Aladdin (Shanghai, China), dissolved
107 in dimethyl sulfoxide (DMSO) at 50 mM and stored at -20 °C. Resveratrol (R5010),
108 NAD⁺ (β-nicotinamide adenine dinucleotide hydrate) (N7004), ATP (A6419),
109 lipopolysaccharide (LPS) (*Escherichia coli* O111:B4) (L4391), Hoechst 33342
110 (B2261), propidium iodide (PI) (P4170), anti-γ-tubulin (T5326), CF647-conjugated
111 anti-mouse IgG (H+L), highly cross-adsorbed (SAB4600183), PMA (S1819), DMSO
112 (D8418) and Tween-20 (P1379) were bought from Sigma-Aldrich (St. Louis, MO,
113 USA). Nigericin (tlrl-nig), Pam3CSK4 (tlrl-pms), Poly(dA:dT) (tlrl-patn), and
114 FLA-PA Ultrapure (purified flagellin from *P. aeruginosa*) (tlrl-pafla) were obtained
115 from InvivoGen (San Diego, CA, USA). Epothilone B (S1364) was purchased from
116 Selleck Chemicals (Houston, TX, USA), dissolved in DMSO at 5 mM and stored at
117 -20 °C. Dulbecco's Modified Eagle's Medium (DMEM) medium with high glucose,
118 Opti-MEM, fetal bovine serum (FBS), streptomycin and penicillin, Lipofectamine
119 2000 (11668-030), and Lipofectamine RNAiMAX (13778-075) were products of
120 ThermoFisher/Invitrogen/Gibco (Carlsbad, CA, USA). FuGENE HD transfection
121 reagent (E2311) was from Promega (Madison, WI, USA). The anti-NLRP3 antibody
122 (AG-20B-0014) was purchased from Adipogen AG (Liestal, Switzerland). The
123 antibody against actin (sc-1616-R) was purchased from Santa Cruz Biotechnology
124 (Dallas, TX, USA). Specific antibodies against IL-1β (#12242), ASC (#67824),
125 ASC-AlexaFluor488 (#17507), α-tubulin (#3873), acetyl-α-tubulin (#5335),
126 horse-radish peroxidase (HRP)-linked horse anti-mouse IgG (#7076) and horse-radish
127 peroxidase (HRP)-linked goat anti-rabbit IgG (#7074) were purchased from Cell
128 Signaling Technology (Danvers, MA, USA). The antibodies against
129 pro-caspase1+p10+p12 (ab179515), GSDMD (ab209845) and MEC-17 (ab58742)
130 were purchased from Abcam (Cambridge, UK). CF568-conjugated goat-anti-rabbit
131 IgG (H+L), highly cross-adsorbed (20103) and CF488A-conjugated goat-anti-mouse
132 IgG, highly cross-adsorbed (20018) were obtained from Biotium (Hayward, CA,
133 USA).

134 **Animals**

135 C57BL/6 mice (6–8 weeks of age) were obtained from the Experimental Animal
136 Center of Southern Medical University (Guangzhou, China). All the mice were
137 acclimatized for one week before experiment.

138 **Mouse J774A.1 macrophages**

139 Mouse J774A.1 macrophage cell line was purchased from the Kunming Cell Bank of
140 Type Culture Collection, Chinese Academy of Sciences (Kunming, China). Cells were
141 cultured in DMEM supplemented with 10% FBS, 100 U/ml penicillin, 100 µg/ml
142 streptomycin and 2 mM L-glutamine (complete DMEM medium) at 37 °C in a
143 humidified incubator of 5% CO₂ and sub-cultured every 2-3 days by using a cell
144 scraper to detach cells.

145 **Bone marrow-derived macrophages (BMDMs)**

146 Mouse BMDMs were isolated and differentiated as reported previously (26,27). In
147 brief, C57BL/6 mice were sacrificed and bone marrow cells in hind femora and tibias
148 were flushed out with 10 ml of sterile PBS and collected by centrifugation at 300 × g
149 for 5 min at 4 °C. Then the cells were re-suspended in BM-Mac medium (80% DMEM
150 medium containing 10% FBS plus 20% M-CSF-conditioned medium from L929 cells)
151 and differentiated for 6 days at 37 °C in a humidified incubator of 5% CO₂. BMDMs
152 were cultured in 24-well plates at 1.5 × 10⁵ cells/well (0.5 ml) or in 6-well plates at
153 1.2 × 10⁶ cells/well (2 ml) or in glass-bottomed dishes at 1 × 10⁵ cells/dish (1.5 ml)
154 with complete DMEM medium at 37 °C overnight, and were ready for experiments.

155 **THP-1 cell culture and differentiation**

156 THP-1 cells (ATCC) were maintained in RPMI-1640 supplemented with 10% FBS
157 and 50 µM 2-mercaptoethanol at 37 °C in a humidified incubator of 5% CO₂. They
158 were differentiated into macrophages by incubation with 500 nM PMA for 16 h, and
159 then were ready for experiments.

160 **Western blot analysis**

161 Western blotting was performed essentially as previously described (26). Briefly, total
162 proteins were separated by sodium dodecylsulfate-polyacrylamide gel electrophoresis

163 (SDS-PAGE) and electro-transferred to PVDF membranes (03010040001; Roche
164 Diagnostics GmbH, Mannheim, Germany). The membranes were blocked by blocking
165 buffer (PBS containing 3% FBS) for 1 h and incubated with indicated primary
166 antibody overnight at 4 °C, followed by incubation with HRP-linked secondary
167 antibody. Bands were revealed with an enhanced chemiluminescence kit (BeyoECL
168 Plus; Beyotime, Shanghai, China) and recorded by X-ray films (Carestream, Xiamen,
169 China). The blot images were captured by FluorChem8000 imaging system
170 (AlphaInnotech, San Leandro, CA, USA). The gray values were analyzed by
171 AlphaEaseFC 4.0 software (AlphaInnotech).

172 **Precipitation of soluble proteins in supernatants**

173 Soluble protein secreted into culture supernatants (equal volume for each sample) was
174 precipitated as previously described (26,27). After washing three times with cold
175 acetone, the precipitated proteins were re-dissolved in equal volume of 2×SDS-PAGE
176 loading buffer, and then secreted mature IL-1 β and caspase-1p10 were analyzed by
177 western blotting.

178 **Detection of soluble IL-1 β**

179 Soluble IL-1 β in culture supernatants and serum were determined by cytometric bead
180 array (CBA) mouse IL-1 β Flex Set (#560232) with the buffer (#558266) or human
181 inflammatory cytokine kit (#551811), respectively (BD Biosciences, San Jose, CA,
182 USA) according to the manufacturer's instructions. Data were acquired on a flow
183 cytometer (Attune NxT acoustic focusing cytometer; Thermo Fisher Scientific,
184 Carlsbad, CA, USA) and analyzed by using the Attune NxT software (Thermo Fisher
185 Scientific).

186 **Immunofluorescence microscopy**

187 Immunofluorescence analysis was performed as previously described (26). In brief,
188 macrophages were seeded in glass-bottomed dishes and cultured at 37 °C overnight.
189 Cells were fixed in 4% paraformaldehyde for 15 min, and permeabilized with 2 ml
190 cold methanol (-20 °C) for 10 min, and then by incubated with primary antibodies at
191 4 °C overnight, followed by staining with CF568-conjugated goat-anti-rabbit IgG and

192 CF488A-conjugated goat-anti-mouse IgG. In separate experiments for simultaneously
193 staining of ASC, acetylated α -tubulin and γ -tubulin, cells were incubated with rabbit
194 anti-acetylated α -tubulin and mouse-anti- γ -tubulin, and then stained with
195 CF647-conjugated anti-mouse IgG and CF568-conjugated goat-anti-rabbit IgG,
196 followed by incubation with ASC-AlexaFluor488. The nuclei were revealed by
197 Hoechst33342 (5 μ g/ml) staining. Cells were observed under a Zeiss Axio Observer
198 D1 microscope with a Zeiss LD Plan-Neofluar 40 \times 0.6 Korr M27 objective lens (Carl
199 Zeiss MicroImaging GmbH, Göttingen, Germany). Fluorescence images were
200 captured by a Zeiss AxioCam MR R3 cooled CCD camera controlled with ZEN
201 software (Carl Zeiss).

202 **Cell Death Assay**

203 Cell death was measured by propidium iodide (PI) incorporation as described
204 previously (26). Briefly, macrophages were cultured in 24-well plates and primed in
205 Opti-MEM with 500 ng/ml LPS for 4 h. Then the cells were treated with indicated
206 concentration of paclitaxel for 1 h followed by stimulation with ATP (2 mM or 3 mM)
207 or nigericin (5 μ M or 20 μ M) for indicated time periods. The nuclei were revealed by
208 Hoechst 33342 (5 μ g/ml) staining. Dying cells revealed by PI (2 μ g/ml) staining at
209 room temperature for 10 min and observed immediately by live imaging using Zeiss
210 Axio Observer D1 microscope equipped with a Zeiss LD Plan-Neofluar 20 \times 0.4 Korr
211 M27 objective lens (Carl Zeiss MicroImaging GmbH, Göttingen, Germany).
212 Fluorescence images were captured with a Zeiss AxioCam MR R3 cooled CCD
213 camera controlled with ZEN software (Carl Zeiss).

214 **Small interfering RNA (siRNA)**

215 The siRNA (5'-GGA TAC AAG AAG CTC TTT G-3') duplexes targeting mouse
216 *MEC-17* (17) and negative control (NC) siRNA were synthesized by RiboBio
217 (Guangzhou, China). Knockdown of *MEC-17* was performed using Lipofectamine
218 RNAiMAX according to the instructions provided by the supplier. Briefly, BMDMs
219 were cultured in 6-well plates at 37 $^{\circ}$ C overnight. The NC siRNA and *MEC-17* siRNA
220 was added to corresponding well at a final concentration of 100 nM. Cells were

221 cultured in DMEM medium containing 10% FBS for 72 h, and used for experiments.

222 **Bacterial infection**

223 Mouse model of bacterial infection was established as previously described (26,28).
224 In brief, *E. coli* DH5 α was cultured and proliferated in Lysogeny broth (LB) medium
225 at 37 °C overnight, and then re-inoculated into fresh LB media and grown for 4 h at
226 37 °C. The viable bacteria were collected by centrifugation at 2600 \times g for 10 min,
227 washed with PBS, and then re-suspended in appropriate volume of PBS. Bacterial
228 density was measured by using an ultraviolet-visible spectrophotometer
229 (NanoDrop2000, Thermo Scientific) and the corresponding colony-forming units
230 (CFUs) were determined on LB agar plates (29). Then the viable bacteria were
231 re-suspended in PBS at 4×10^9 CFU/ml. C57BL/6 mice were acclimated for a week,
232 randomly divided into three groups and intraperitoneally injected with paclitaxel
233 solution (5 or 10 mg/kg body weight) or vehicle (PBS). One hour later, viable *E. coli*
234 cells (2×10^9 CFU/mouse) in 0.5 ml of PBS were injected into the peritoneal cavity of
235 each mouse. Mouse survival was monitored every 6 h for five consecutive days. In a
236 paralleled experiment, mice were intraperitoneally injected with paclitaxel solution
237 similarly. One hour later, viable *E. coli* cells (1×10^9 CFU/mouse) in 0.5 ml of PBS
238 were injected into the peritoneal cavity of each mouse and those mice were sacrificed
239 at 8 h post bacterial infection. Their sera were collected for detection of IL-1 β by
240 CBA.

241 **Histopathological analysis**

242 Infected mice were sacrificed and the livers were isolated and fixed in 4% neutral
243 formaldehyde, and the liver sections were stained with hematoxylin and eosin (H&E).
244 Images were captured by the Zeiss Axio Observer D1 microscope armed with a color
245 CCD (Zeiss Axio Observer D1).

246 **Statistical Analysis**

247 Experiments were performed three times independently. Data were expressed as mean
248 \pm standard deviation (SD). Statistical analysis was performed using GraphPad
249 Prism7.0 (GraphPad Software Inc, San Diego, CA, United States). One-way analysis

250 of variance (ANOVA) followed by Turkey post hoc test and unpaired Student's t-test
251 were used to analyze the statistical significance among multiple groups and between
252 two groups, respectively. If the data were not normally distributed, Friedman (among
253 multiple groups) and Mann-Whitney U (between two groups) were used, respectively.
254 Kaplan–Meier survival curves were used for analysis of mouse survival and the
255 significance was evaluated by the log-rank (Mantel–Cox) test. *P*-value < 0.05 was
256 considered statistically significant.

257

258 **RESULTS**

259 **Paclitaxel promotes NLRP3 inflammasome activation in murine** 260 **macrophages**

261 As colchicine acting as a microtubule-destabilizing agent can suppress NLRP3
262 inflammasome activation (17,20), we asked whether paclitaxel, a
263 microtubule-stabilizing agent, could influence NLRP3 inflammasome activation. To
264 explore this problem, we assessed the effects of paclitaxel on NLRP3 inflammasome
265 activation in LPS-primed murine J774A.1 or bone marrow-derived macrophages
266 (BMDMs) stimulated with extracellular ATP or nigericin, two canonical NLRP3
267 inflammasome activators (30). Western blot analysis showed that LPS priming
268 upregulated the expression of NLRP3 and pro-IL-1 β proteins (**Figure 1**). Upon ATP
269 or nigericin stimulation, cleaved caspase-1p10 (10 kDa) and mature IL-1 β (17 kDa)
270 were detectable in the culture supernatants of macrophages, indicative of the
271 activation of NLRP3 inflammasome. Interestingly, paclitaxel dose-dependently
272 increased the release of cleaved caspase-1p10 and mature IL-1 β into the culture
273 supernatants of J774A.1 cells stimulated with ATP (**Figure 1A-C**) and of BMDMs
274 stimulated with ATP (**Figure 1D-F**) or nigericin (**Figure 1G-I**), indicating that this
275 chemical enhanced NLRP3 inflammasome activation in murine macrophages.
276 Paclitaxel also promoted the activation of non-canonical NLRP3 inflammasome
277 induced by transfecting LPS into macrophages primed with TLR1/2 agonist
278 Pam3CSK4 (**Supplementary Figures S1 and S2**). However, NLRC4 (activated by

279 flagellin transfection) or AIM2 (activated by poly(dA:dT) transfection) inflammasome
280 activation in Pam3CSK4-primed macrophages were unaffected by paclitaxel
281 pretreatment (**Supplementary Figure S1 and S2**). Together, these results showed that
282 paclitaxel specifically potentiated both canonical and non-canonical NLRP3
283 inflammasome activation in murine macrophages.

284

285 **Paclitaxel increases ASC speck formation in BMDMs upon NLRP3** 286 **inflammasome activation**

287 The assembly and activation of NLRP3 inflammasome requires a key adapter
288 protein named apoptosis-associated speck-like protein containing a caspase
289 recruitment domain (ASC). During the assembly of NLRP3 inflammasome, ASC
290 forms one large speck in each cell by self-oligomerization, which becomes another
291 marker of NLRP3 inflammasome activation (13). To confirm the aforementioned
292 results obtained from Western blot analysis (**Figure 1**), we next explored whether
293 paclitaxel increased ASC speck formation induced by ATP. Immunofluorescence
294 microscopy analysis showed that ASC distributed evenly in LPS-primed BMDMs, but
295 upon ATP stimulation, ASC specks were observed in ~ 35% of the cells (**Figure 2A,**
296 **B**). Paclitaxel pretreatment greatly increased the numbers of ASC speck induced by
297 ATP stimulation, and in ~85% of the cells each contained one ASC speck near the
298 nucleus (**Figure 2A**), corroborating that paclitaxel promoted NLRP3 activation in
299 macrophages. These results also suggested that paclitaxel enhanced NLRP3 activation
300 by promoting the assembly of NLRP3 with ASC.

301

302 **Paclitaxel enhances ATP- or nigericin-induced pyroptosis in** 303 **macrophages**

304 Active caspase-1 cleaves GSDMD to produce a GSDMD-NT fragment, which
305 binds to and forms pores in the plasma membrane, leading to loss of membrane
306 integrity and a rapid programmed cell death named pyroptosis (15,23). The pyroptotic
307 cell death is a form of necrosis that can be revealed by propidium iodide (PI) staining.

308 Therefore, we next explored whether paclitaxel could enhance ATP- or
309 nigericin-induced pyroptosis. Consistent with enhanced NLRP3 activation (**Figures 1**
310 and **Figures 2A, B**), paclitaxel dose-dependently increased ATP-induced generation
311 of GSDMD-NT (32 kDa) (**Figures 2C, D**). Concurrent with the production of
312 GSDMD-NT, ~20% of BMDMs were undergoing lytic cell death upon ATP
313 stimulation, and paclitaxel dose-dependently increased the cell death (**Figures 2E, F**
314 and **Supplementary Figure S3A**). The dying cells displayed cell swelling and
315 membrane ballooning (**Figure 2F**), mirroring the morphological characteristics of
316 pyroptosis. Similarly, paclitaxel also dose-dependently increased lytic cell death and
317 GSDMD cleavage upon nigericin stimulation in LPS-primed BMDMs
318 (**Supplementary Figures S3B-D**) or upon ATP stimulation in LPS-primed J774A.1
319 cells (**Supplementary Figures S4A-C**). All these results indicated that paclitaxel
320 promoted NLRP3 inflammasome activation and pyroptosis induced by ATP or
321 nigericin treatment, suggesting its potential in enhancing the innate immune response.

322

323 **Paclitaxel dose- and time-dependently induces α -tubulin acetylation**

324 We next sought to explore how paclitaxel enhanced NLRP3 inflammasome activation.
325 Acetylation of α -tubulin in microtubules has been shown to be critical for ASC
326 trafficking and the assembly of NLRP3 inflammasome (17) while paclitaxel has been
327 shown to induce α -tubulin acetylation (24). We thus assayed whether paclitaxel
328 affected α -tubulin acetylation in LPS-primed macrophages. Western blotting showed
329 that paclitaxel markedly elevated the levels of acetylated α -tubulin in J774A.1
330 macrophage (**Figures 3A, B**) and BMDMs in dose- or time-dependent manner
331 (**Figures 3C-F**), but did not change the levels of total α -tubulin. In addition,
332 paclitaxel-induced acetylation of α -tubulin occurred within 15 min and quickly
333 reached the plateau at 30 min (**Figures 3E, F**). Although the levels of α -tubulin
334 acetylation in paclitaxel plus ATP or nigericin groups were not further increased as
335 compared to paclitaxel alone, they were much higher than that of ATP or nigericin
336 alone (**Supplementary Figure S5**). Enhanced α -tubulin acetylation and NLRP3

337 inflammasome activation (as indicated by IL-1 β release) by paclitaxel were
338 corroborated in human THP-1 macrophages (**Supplementary Figure S6**). Together,
339 these results indicated that paclitaxel rapidly and markedly induced α -tubulin
340 acetylation in macrophages, suggesting its involvement in enhanced NLRP3
341 inflammasome activation.

342 **Blockade of α -tubulin acetylation attenuates paclitaxel-mediated** 343 **augmentation of NLRP3 inflammasome activation**

344 To corroborate the involvement of increased α -tubulin acetylation in mediating
345 paclitaxel-induced augmentation of NLRP3 inflammasome activation, we used
346 pharmacologic agents to block the acetylation of α -tubulin. Immunofluorescence
347 microscopy showed that paclitaxel, nigericin or their combination induced formation
348 of clusters of acetylated α -tubulin in BMDMs, which were distributed near the
349 perinuclear region of the cell (**Figure 4A**). Such increased acetylation of α -tubulin
350 was markedly suppressed by resveratrol or NAD⁺ (**Figures 4A, B**), two activators of
351 NAD⁺-dependent deacetylases Sirt1/Sirt2 (31,32). Concomitant with the suppression
352 of α -tubulin acetylation, ATP-induced ASC speck formation was significantly
353 decreased by resveratrol, either in the presence or absence of paclitaxel (**Figures 4C,**
354 **D, and Supplementary Figure S7**). Similarly, paclitaxel-induced increase of soluble
355 IL-1 β release in the culture supernatants was also suppressed by resveratrol or NAD⁺
356 (**Figures 4E**), indicating that these two agents attenuated NLRP3 inflammasome
357 activation in macrophages. Interestingly, accompanying the increase of α -tubulin
358 acetylation, paclitaxel pretreatment enhanced the co-localization of ASC specks with
359 the acetylated α -tubulin and centrioles (revealed by γ -tubulin), whereas resveratrol
360 was able to reverse this process, with fewer ASC specks being co-located with the
361 acetylated α -tubulin and centrioles (**Figure 5**), suggesting that the apposition of ASC
362 speck and γ -tubulin was mediated by acetylated α -tubulin, and that paclitaxel
363 promoted such a process. Together, these results verified the involvement of
364 paclitaxel-induced α -tubulin acetylation in enhancing NLRP3 inflammasome
365 activation probably by facilitating the assembly of ASC speck.

366

367 **The acetyltransferase MEC-17 participates in paclitaxel-mediated**
368 **acetylation of α -tubulin and augmentation of NLRP3 inflammasome**
369 **activation**

370 Published studies have shown that MEC-17 (also known as α -tubulin
371 acetyltransferase 1, α TAT1) is responsible for the acetylation of α -tubulin (33,34),
372 thus being involved in NLRP3 inflammasome activation (17). To test whether
373 MEC-17 was involved in paclitaxel-mediated augmentation of NLRP3 activation, we
374 knocked down *MEC-17* expression by using siRNA. Western blot analysis showed
375 that the expression of MEC-17 was decreased by ~90% after siRNA knockdown of
376 *MEC-17* as compared to negative control (**Figures 6A, B**). As expected, *MEC-17*
377 knockdown markedly suppressed the levels of both basal (without paclitaxel treatment)
378 and paclitaxel-induced α -tubulin acetylation in LPS-primed J774A.1 cells (**Figures**
379 **6C, D**). Immunofluorescence microscopy also revealed that paclitaxel-induced
380 α -tubulin acetylation was markedly attenuated by *MEC-17* siRNA as compared to NC
381 siRNA treatment in LPS-primed J774A.1 and BMDM cells, whereas α -tubulin
382 distribution was largely unaffected (**Figures 6E, F**). Furthermore, NLRP3 activation
383 (indicated by IL-1 β release) and lytic cell death (indicated by PI staining) was induced
384 by ATP in J774A.1 cells, but was significantly suppressed in those cells with *MEC-17*
385 knockdown, either in the presence or absence of paclitaxel (**Figures 6G, H**). Similarly,
386 *MEC-17* knockdown significantly suppressed nigericin-induced soluble IL-1 β release
387 and cell death in LPS-primed BMDMs, either in the presence or absence of paclitaxel
388 (**Figures 6I, J**). Together, these results indicated that MEC-17 was involved in
389 paclitaxel-induced augmentation of NLRP3 inflammasome activation by increasing
390 acetylation of α -tubulin.

391

392 **Epothilone B, like paclitaxel, does not influence macrophage priming but**
393 **does enhance NLRP3 inflammasome activation**

394 Next, we explored whether epothilone B, another microtubule-stabilizing drug

395 that is functionally similar to paclitaxel but has a distinct molecular structure (37),
396 also enhanced NLRP3 inflammasome activation. The results showed that, similar to
397 paclitaxel, single epothilone B did not induce the expression of pro-IL-1 β and NLRP3
398 in unprimed BMDMs (**Figure 7A**), but it evidently enhanced pyroptosis (**Figures**
399 **7B,C**) and IL-1 β release (indicative of NLRP3 inflammasome activation) (**Figure 7D**)
400 in LPS-primed BMDMs. Interestingly, epothilone B also dose-dependently induced
401 α -tubulin acetylation in LPS-primed BMDMs (**Supplementary Figure S8**),
402 suggesting that epothilone B and paclitaxel shared a common mechanism in
403 enhancing NLRP3 inflammasome activation.

404 Previous studies showed that paclitaxel was an LPS mimetic that can bind with
405 Toll-like receptor 4 (TLR4) to induce MyD88/NF- κ B signaling (35,36). However, it is
406 unclear whether this activity of paclitaxel accounts for its action in enhancing NLRP3
407 inflammasome activation and pyroptosis. To clarify this issue, we first explored
408 whether paclitaxel had a similar effect like LPS in priming macrophages. Western blot
409 analysis showed that LPS induced the expression of pro-IL-1 β and NLRP3 that are
410 requisite for NLRP3 inflammasome assembly but paclitaxel did not (**Figure 7**),
411 indicating that paclitaxel had no macrophage-priming activity in the process of
412 inflammasome activation.

413

414 **Paclitaxel administration enhances the innate immune response against** 415 **bacterial infection in mice**

416 As NLRP3 inflammasome activation represents critical innate defense
417 mechanism against bacterial infection (38), we next explored the functional relevance
418 of paclitaxel-mediated augmentation of NLRP3 activation in a mouse model of
419 bacterial infection. To this end, mice were intraperitoneally injected with paclitaxel (5
420 and 10 mg/kg body weight) or vehicle (PBS) 1 h before peritoneal injection with a
421 lethal dose of viable *E. coli* (2×10^9 CFU/mouse). All vehicle-treated mice were
422 succumbed to such a lethal dose of *E. coli* infection within 24 h, whereas ~10% (in 5
423 mg/kg paclitaxel group) and 50% (in 10 mg/kg paclitaxel group) of paclitaxel-treated

424 mice survived the experimental period of observation (120 h), respectively (**Figure**
425 **8A**). In a parallel experiment, the peritoneal bacterial burden and IL-1 β levels in the
426 serum were evaluated at 8 h post infection. The bacterial burden in the peritoneal
427 fluids was significantly reduced in paclitaxel group as compared to vehicle group
428 (**Figure 8B**). Moreover, paclitaxel administration significantly increased the serum
429 levels of IL-1 β in the mouse model of bacterial infection (**Figure 8C**). Consistent with
430 reduced bacterial burden and increased mouse survival, paclitaxel-treated mice
431 displayed decreased infiltration of inflammatory cells in the liver as compared with
432 vehicle group (**Figure 8D**). These results indicated that paclitaxel potentiated the
433 innate immune response against bacterial infection probably by increasing NLRP3
434 inflammasome activation *in vivo* in mice.

435

436 **DISCUSSION**

437 It has been demonstrated that paclitaxel can ameliorate LPS-induced kidney
438 injury and improve animal survival in a mouse model of LPS-induced sepsis (39,40).
439 Paclitaxel can also attenuate sepsis-induced liver injury (41). Although some studies
440 have implicated paclitaxel in regulating NLRP3 inflammasome activation (25), the
441 underlying mechanism has not been completely elucidated. In this study, we
442 demonstrated that paclitaxel enhanced NLRP3 inflammasome activation and
443 pyroptosis, leading to increased IL-1 β release and enhanced anti-bacterial response *in*
444 *vivo*. Consistent with this, paclitaxel treatment significantly improved animal survival
445 in a mouse model of bacterial infection. Such immunomodulatory activity of
446 paclitaxel suggests its potential application, beyond in cancer therapy, in infectious
447 diseases.

448 Intriguingly, the assembly of NLRP3 inflammasome relies on the cargo
449 trafficking machinery of microtubule tracks (17,18). Microtubules are composed of α -
450 and β -tubulin subunits, serving as a major cytoskeleton to maintain cell morphology.
451 They are also tracks for cargo trafficking (42). Several manners of microtubule
452 post-translational modifications have been reported (43). For example, the α -subunit

453 can be acetylated by α -tubulin acetyltransferase 1 (α TAT1/MEC-17) at lysine 40,
454 which is located inside the microtubule (33, 43), while SIRT2 serves as an α -tubulin
455 deacetylase (44). Although acetylation of α -tubulin does not change the assembly and
456 morphology of microtubules, it increases the mechanical stability and flexibility of the
457 microtubules, accelerating their shrinkage and thus promoting vesicle transport (45).
458 Upon α -tubulin acetylation, microtubules tend to form bundles, which enhance the
459 motor functions of dynein and kinesin in transporting cargoes (46,47). During the
460 assembly of NLRP3 inflammasome, the adaptor protein ASC is located on
461 mitochondria that are transported as cargoes along the microtubule to the minus end,
462 where the centrioles dwell, forming the mitochondrion associated ER membrane
463 (MAM) (17). In line with this, the apposition of NLRP3 specks, γ -tubulin (indicative
464 of centrioles) and the microtubule-affinity regulating kinase 4 (MARK4), a
465 microtubule-associated protein (MAP) regulating microtubule dynamics, has been
466 observed upon NLRP3 inflammasome activation (18). Interestingly, α -tubulin is
467 acetylated upon ATP and nigericin treatment, while the NAD^+ -dependent deacetylase
468 SIRT2 was suppressed by them due to reduced NAD^+ concentration in this process
469 (17). Two activators of SIRT2, resveratrol and NAD^+ , suppress the approximation of
470 ASC to NLRP3, thus inhibiting the assembly of NLRP3 inflammasome (48).
471 Therefore, α -tubulin acetylation seems necessary for the trafficking of inflammasome
472 components including ASC to the perinuclear region, thus accelerating NLRP3
473 inflammasome assembly. Consistent with previous studies(24), we demonstrated that
474 paclitaxel is a strong inducer of α -tubulin acetylation as a low concentration of
475 paclitaxel (0.4 nM) was sufficient to induce α -tubulin acetylation in LPS-primed
476 macrophages (see **Figure 3**). Based on the studies mentioned above together with our
477 observation, we proposed that induction of α -tubulin acetylation by paclitaxel
478 facilitated the assembly of NLRP3 inflammasome. Indeed, paclitaxel treatment led to
479 increased formation of ASC specks upon ATP or nigericin stimulation, and most of
480 the ASC specks were observed apposition with γ -tubulin, whereas inhibition of the
481 α -tubulin acetylation by inhibitors (NAD^+ or resveratrol) greatly reduced the ASC
482 speck formation induced by paclitaxel plus ATP (see **Figure 4A and 5**). This was

483 likely due to that resveratrol and NAD^+ prevented the minus end-oriented trafficking
484 of ASC along the microtubule track by decreasing α -tubulin acetylation, thus
485 preventing the apposition of ASC specks with γ -tubulin. In line with the reduction of
486 ASC specks, paclitaxel-augmented NLRP3 inflammasome activation was also
487 inhibited by resveratrol, NAD^+ , or *MEC-17* siRNA knockdown. Our data suggest that
488 acetylated α -tubulin-mediated apposition of ASC and γ -tubulin is required for NLRP3
489 inflammasome activation, and that paclitaxel, via inducing α -tubulin acetylation,
490 promotes ASC trafficking and speck formation during the assembly of NLRP3
491 inflammasome.

492 Although paclitaxel strongly induces α -tubulin acetylation as revealed by
493 previous studies (24) and ours, the underlying mechanism is not fully elucidated.
494 Previous reports have indicated that paclitaxel binds to β -tubulin and stabilize the
495 microtubule (49). As the lysine 40 residue is buried inside the lumen of microtubule,
496 paclitaxel binding to the microtubule may make the α TAT1 easier to access the lumen
497 (lysine 40), thus leading to increased acetylation of α -tubulin. Alternatively, paclitaxel
498 may block the deacetylation process by SIRT2 via yet-unknown mechanism.
499 Interestingly, previous reports have indicated that berberine also induces α -tubulin
500 acetylation in tumor cells (50). However, berberine did not induce α -tubulin
501 acetylation in the context of our experiment (i.e., in LPS-primed macrophages, **data**
502 **not shown**) at the concentrations that enhance NLRP3 inflammasome activation as
503 revealed by us previously (51). Several studies have indicated that paclitaxel induces
504 mitochondrial reactive oxidative species (ROS) (52), which is an inducer of α -tubulin
505 acetylation (53). Interestingly, paclitaxel in combination of lentinan (a polysaccharide
506 isolated from mushroom) triggers ROS production in A549 cells and enhances
507 apoptosis by activating ROS-TXNIP-NLRP3 inflammasome (54). These studies
508 suggest that paclitaxel enhanced the NLRP3 inflammasome activation by induction of
509 ROS, although paclitaxel-induced ROS (if there was) was not detected in the present
510 study. Indeed, reducing ROS production by resveratrol has contributed to its action to
511 suppress NLRP3 inflammasome activation (48). There are also studies indicating that
512 paclitaxel is an LPS mimetic, which binds to MD-2/TLR-4 and results in the

513 activation or suppression of NF- κ B activation (40). However, our data showed that
514 paclitaxel *per se* did not induce the expression of NLRP3 and pro-IL-1 β (indicators of
515 macrophage priming) as LPS does, nor did it influence the levels of these proteins
516 induced by LPS (see **Figure 1**). Moreover, paclitaxel did not influence the AIM2 and
517 NLRC4 inflammasome activation induced by poly(dA:dT) and flagellin, respectively.
518 Interestingly, epothilone B, another microtubule-stabilizing molecular like paclitaxel
519 but with a distinct molecular structure (37), showed similar activities as paclitaxel in
520 enhancing pyroptosis and IL-1 β release as well as inducing α -tubulin acetylation in
521 LPS-primed macrophages. Therefore, it is unlikely that paclitaxel enhanced NLRP3
522 inflammasome activation by increased macrophage priming, but by sharing a
523 common mechanism with epothilone B to induce α -tubulin acetylation.

524 Interestingly, in contrast to the action of paclitaxel, colchicine has been shown to
525 suppress NLRP3 inflammasome activation in macrophages stimulated by nigericin,
526 ATP or monosodium urate crystal (MSU) (17, 20). Mechanistically, colchicine
527 inhibited the activation of NLRP3 inflammasome by decreasing the levels of
528 acetylated α -tubulin induced by the stimulators (17). These studies have explained the
529 pharmacological action of colchicine in clinical treatment of gout (55), an
530 inflammatory disease induced by MSU (20). Indeed, the anti-gout activity of
531 colchicine is likely due to suppression of the inflammasome activation by MSU (21).
532 Considering that colchicine is a microtubule-destabilizing agent (56) while paclitaxel
533 being a microtubule-stabilizing agent (24), the above-mentioned studies together with
534 our present data suggest that targeting microtubules may either suppress or booster
535 NLRP3 inflammasome activation in terms of differential actions on the microtubule
536 cytoskeleton.

537 Previous studies have indicated that full activation of NLRP3 inflammasome is
538 required for efficient elimination of invaded pathogens, and loss of the NLRP3
539 inflammasome machinery, including genetic deficiency of *IL-1r*, *caspase-1* and/or *-11*,
540 aggravates the infectious diseases and increases animal death (57). Mice with both
541 *caspase-1* and *-11* deficiencies, thus lacking mature IL-1 β and IL-18, lose the capacity
542 to recruit neutrophils and natural killer (NK) cells to the infectious site, and they can

543 even succumb to common environmental bacteria (58). Mature IL-1 β is produced by
544 active caspase-1 upon inflammasome activation and it is a strong chemoattractant for
545 neutrophils, one of the most important immune cells that engulf and kill pathogens
546 (59). By binding to the receptor IL-1R, IL-1 β participates in macrophage
547 differentiation and activation (60), increasing their capacity for presenting pathogenic
548 antigens to T lymphocytes (61). It also stimulates T lymphocytes to differentiate into
549 T helper (Th) 17/Th1 cells (62) and is required for B cell activation, proliferation and
550 antibody production (63). Therefore, increased IL-1 β secretion by paclitaxel upon
551 inflammatory stimuli, suggestive of enhanced innate and adaptive immunity, is likely
552 beneficial for bacterial clearance. Indeed, our study revealed that paclitaxel promoted
553 the clearance of bacteria and improved animal survival, accompanied by alleviated
554 infiltration of inflammatory cells in the liver. In further support of this notion, we have
555 reported that another Chinese herbal ingredient berberine with similar activities to
556 paclitaxel in enhancing NLRP3 inflammasome activation exhibited significant
557 anti-bacterial activity through enhancing the innate immunity of the host (51).
558 Therefore, augmentation of NLRP3 inflammasome activation by paclitaxel via
559 inducing α -tubulin acetylation makes it potential to be developed as a new
560 antimicrobial and immunomodulatory medicine.

561 As a chemotherapeutic agent, paclitaxel can induce many side effects, including
562 hair loss, bone marrow suppression, numbness, allergic reactions, muscle pains,
563 diarrhea, heart problems, increased risk of infection, and lung inflammation (64, 65).
564 But the doses used in clinic seem higher than those used in our study. More
565 importantly, paclitaxel alone neither induced NLRP3 inflammasome activation nor
566 caused cell death in LPS-primed macrophages. Besides, our experiment showed that
567 paclitaxel did not induce acute tissue damage in mice without bacterial infection
568 (**Figure 9D**). Therefore, the side effects of paclitaxel in clinic may not relate to its
569 activity in enhancing NLRP3 activation.

570 In summary, we demonstrated that paclitaxel was able to potentiate innate
571 immune responses, including NLRP3 inflammasome activation, IL-1 β release and
572 pyroptosis, reducing bacterial burden and improving animal survival. The data

573 suggest that paclitaxel may have potential application in combating pathogenic
574 infection and other inflammatory diseases. In particular, this property of paclitaxel
575 suggests its potential application in treatment of sustained infection-related lesions
576 such as sores, furuncle and beriberi. Further investigation is warranted to verify the *in*
577 *vivo* effects of paclitaxel in appropriate pre-clinical animal models of such diseases.

578 **ETHICS STATEMENT**

579 All animal experiments were performed according to the guidelines for the care and
580 use of animals approved by the Committee on the Ethics of Animal Experiments of
581 Jinan University.

582 **AUTHOR CONTRIBUTIONS**

583 Q.Zeng, F.Y., C.L., and L.X. performed *in vitro* studies; C.L., L.X., F.M., C.Zeng, and
584 C.Zhang conducted animal studies; C.L. and Q.Z. analyzed the data; D.O., Q.Zha and
585 X.H. supervised the study; D.O. and X.H. wrote the paper.

586 **FUNDING**

587 This work was supported by the grants from the National Natural Science Foundation
588 of China (No. 81873064, No. 81773965 and No. 81673664).

589 **SUPPLEMENTARY MATERIAL**

590 The Supplementary Material for this article can be found online.

591 **REFERENCES:**

- 592 1. Gupta N, Hatoum H and Dy GK. First line treatment of advanced non-small-cell
593 lung cancer - specific focus on albumin bound paclitaxel. *Int J Nanomedicine*.
594 (2014) 9:209-21. doi:10.2147/ijn.s41770
- 595 2. Perez EA. Paclitaxel in Breast Cancer. *Oncologist*. (1998) 3:373-89.
- 596 3. Blair HA and Deeks ED. Albumin-Bound Paclitaxel: A Review in Non-Small Cell
597 Lung Cancer. *Drugs*. (2015) 75:2017-24. doi:10.1007/s40265-015-0484-9
- 598 4. Vassileva V, Allen CJ and Piquette-Miller M. Effects of sustained and intermittent
599 paclitaxel therapy on tumor repopulation in ovarian cancer. *Mol Cancer Ther*.
600 (2008) 7:630-7. doi:10.1158/1535-7163.mct-07-2117

- 601 5. de Weger VA, Beijnen JH and Schellens JH. Cellular and clinical pharmacology of
602 the taxanes docetaxel and paclitaxel--a review. *Anticancer Drugs*. (2014)
603 25:488-94. doi:10.1097/cad.0000000000000093
- 604 6. De Brabander M, Geuens G, Nuydens R, Willebrords R and De Mey J. Taxol
605 induces the assembly of free microtubules in living cells and blocks the organizing
606 capacity of the centrosomes and kinetochores. *Proc Natl Acad Sci U S A*. (1981)
607 78:5608-612.
- 608 7. Lowe J, Li H, Downing KH and Nogales E. Refined structure of alpha beta-tubulin
609 at 3.5 A resolution. *J Mol Biol*. (2001) 313:1045-57. doi:10.1006/jmbi.2001.5077
- 610 8. Gangemi RM, Tiso M, Marchetti C, Severi AB and Fabbi M. Taxol cytotoxicity on
611 human leukemia cell lines is a function of their susceptibility to programmed cell
612 death. *Cancer Chemother Pharmacol*. (1995) 36:385-92. doi:10.1007/bf00686187
- 613 9. Milas L, Hunter NR, Kurdoglu B, Mason KA, Meyn RE, Stephens LC, et al.
614 Kinetics of mitotic arrest and apoptosis in murine mammary and ovarian tumors
615 treated with taxol. *Cancer Chemother Pharmacol*. (1995) 35:297-303.
616 doi:10.1007/bf00689448
- 617 10. Varbiro G, Veres B, Gallyas F, Jr. and Sumegi B. Direct effect of Taxol on free
618 radical formation and mitochondrial permeability transition. *Free Radic Biol Med*.
619 (2001) 31:548-58.
- 620 11. Ganguly A, Yang H and Cabral F. Paclitaxel-dependent cell lines reveal a novel
621 drug activity. *Mol Cancer Ther*. (2010) 9:2914-23.
622 doi:10.1158/1535-7163.mct-10-0552
- 623 12. Kingsbury SR, Conaghan PG and McDermott MF. The role of the NLRP3
624 inflammasome in gout. *J Inflamm Res*. (2011) 4:39-49. doi:10.2147/jir.s11330
- 625 13. Elliott EI and Sutterwala FS. Initiation and perpetuation of NLRP3
626 inflammasome activation and assembly. *Immunol Rev*. (2015) 265:35-52.
627 doi:10.1111/imr.12286
- 628 14. Jo EK, Kim JK, Shin DM and Sasakawa C. Molecular mechanisms regulating
629 NLRP3 inflammasome activation. *Cell Mol Immunol*. (2016) 13:148-59.
630 doi:10.1038/cmi.2015.95

- 631 15. Shi J, Zhao Y, Wang K, Shi X, Wang Y, Huang H, et al. Cleavage of GSDMD by
632 inflammatory caspases determines pyroptotic cell death. *Nature*. (2015) 526:660-5.
633 doi:10.1038/nature15514
- 634 16. He WT, Wan H, Hu L, Chen P, Wang X, Huang Z, et al. Gasdermin D is an
635 executor of pyroptosis and required for interleukin-1beta secretion. *Cell Res*. (2015)
636 25:1285-98. doi:10.1038/cr.2015.139
- 637 17. Misawa T, Takahama M, Kozaki T, Lee H, Zou J, Saitoh T, et al.
638 Microtubule-driven spatial arrangement of mitochondria promotes activation of the
639 NLRP3 inflammasome. *Nat Immunol*. (2013) 14:454-60. doi:10.1038/ni.2550
- 640 18. Li X, Thome S, Ma X, Amrute-Nayak M, Finigan A, Kitt L, et al. MARK4
641 regulates NLRP3 positioning and inflammasome activation through a
642 microtubule-dependent mechanism. *Nat Commun*. (2017) 8:15986.
643 doi:10.1038/ncomms15986
- 644 19. Yue QX, Liu X and Guo DA. Microtubule-binding natural products for cancer
645 therapy. *Planta Med*. (2010) 76:1037-43. doi:10.1055/s-0030-1250073
- 646 20. Martinon F, Petrilli V, Mayor A, Tardivel A and Tschopp J. Gout-associated uric
647 acid crystals activate the NALP3 inflammasome. *Nature*. (2006) 440:237-41.
648 doi:10.1038/nature04516
- 649 21. Dalbeth N, Lauterio TJ and Wolfe HR. Mechanism of action of colchicine in the
650 treatment of gout. *Clin Ther*. (2014) 36:1465-79.
651 doi:10.1016/j.clinthera.2014.07.017
- 652 22. Gao W, Yang J, Liu W, Wang Y and Shao F. Site-specific phosphorylation and
653 microtubule dynamics control Pyrin inflammasome activation. *Proc Natl Acad Sci*
654 *U S A*. (2016) 113:E4857-66. doi:10.1073/pnas.1601700113
- 655 23. Demidowich AP, Davis AI, Dedhia N and Yanovski JA. Colchicine to decrease
656 NLRP3-activated inflammation and improve obesity-related metabolic
657 dysregulation. *Med Hypotheses*. (2016) 92:67-73. doi:10.1016/j.mehy.2016.04.039
- 658 24. Xiao H, Verdier-Pinard P, Fernandez-Fuentes N, Burd B, Angeletti R, Fiser A, et
659 al. Insights into the mechanism of microtubule stabilization by Taxol. *Proc Natl*
660 *Acad Sci U S A*. (2006) 103:10166-73. doi:10.1073/pnas.0603704103

- 661 25. Jia M, Wu C, Gao F, Xiang H, Sun N, Peng P, et al. Activation of NLRP3
662 inflammasome in peripheral nerve contributes to paclitaxel-induced neuropathic
663 pain. *Mol Pain*. (2017) 13:1744806917719804. doi:10.1177/1744806917719804
- 664 26. Li CG, Yan L, Mai FY, Shi ZJ, Xu LH, Jing YY, et al. Baicalin Inhibits
665 NOD-Like Receptor Family, Pyrin Containing Domain 3 Inflammasome
666 Activation in Murine Macrophages by Augmenting Protein Kinase A Signaling.
667 *Front Immunol*. (2017) 8:1409. doi:10.3389/fimmu.2017.01409
- 668 27. Kayagaki N, Warming S, Lamkanfi M, Vande Walle L, Louie S, Dong J, et al.
669 Non-canonical inflammasome activation targets caspase-11. *Nature*. (2011)
670 479:117-21. doi:10.1038/nature10558
- 671 28. Wegiel B, Larsen R, Gallo D, Chin BY, Harris C, Mannam P, et al. Macrophages
672 sense and kill bacteria through carbon monoxide-dependent inflammasome
673 activation. *J Clin Invest*. (2014) 124:4926-40. doi:10.1172/jci72853
- 674 29. Widdel F. Theory and measurement of bacterial growth. *Grundpraktikum*
675 *Mikrobiologie* (2010) vol. 4. <https://www.mpi-bremen.de/Binaries/Binary307>.
- 676 30. Mariathasan S, Weiss DS, Newton K, McBride J, O'Rourke K, Roose-Girma M,
677 et al. Cryopyrin activates the inflammasome in response to toxins and ATP. *Nature*.
678 (2006) 440:228-32. doi:10.1038/nature04515
- 679 31. Villalba JM and Alcain FJ. Sirtuin activators and inhibitors. *Biofactors*. (2012)
680 38:349-59. doi:10.1002/biof.1032
- 681 32. Pan Y, Zhang H, Zheng Y, Zhou J, Yuan J, Yu Y, et al. Resveratrol Exerts
682 Antioxidant Effects by Activating SIRT2 To Deacetylate Prx1. *Biochemistry*. (2017)
683 56:6325-28. doi:10.1021/acs.biochem.7b00859
- 684 33. Akella JS, Wloga D, Kim J, Starostina NG, Lyons-Abbott S, Morrissette NS, et al.
685 MEC-17 is an alpha-tubulin acetyltransferase. *Nature*. (2010) 467:218-22.
686 doi:10.1038/nature09324
- 687 34. Shida T, Cueva JG, Xu Z, Goodman MB and Nachury MV. The major
688 alpha-tubulin K40 acetyltransferase alphaTAT1 promotes rapid ciliogenesis and
689 efficient mechanosensation. *Proc Natl Acad Sci U S A*. (2010) 107:21517-22.
690 doi:10.1073/pnas.1013728107

- 691 35. Kawasaki K, Gomi K, Kawai Y, Shiozaki M, Nishijima M. Molecular basis for
692 lipopolysaccharide mimetic action of Taxol and flavolipin. *J Endotoxin Res.* (2003)
693 9:301-7 doi:10.1179/096805103225002548
- 694 36. Byrd-Leifer CA, Block EF, Takeda K, Akira S, Ding A. The role of MyD88 and
695 TLR4 in the LPS-mimetic activity of Taxol. *Eur J Immunol.* (2001) 31:2448-57
696 doi:10.1002/1521-4141(200108)31:8<2448::aid-immu2448>3.0.co;2-n
- 697 37. Muhlradt PF, Sasse F. Epothilone B stabilizes microtubuli of macrophages like
698 taxol without showing taxol-like endotoxin activity. *Cancer Res.* (1997) 57:3344-6
- 699 38. Kanneganti TD, Lamkanfi M and Nunez G. Intracellular NOD-like receptors in
700 host defense and disease. *Immunity.* (2007) 27:549-59.
701 doi:10.1016/j.immuni.2007.10.002
- 702 39. Mirzapoiazova T, Kolosova IA, Moreno L, Sammani S, Garcia JG and Verin AD.
703 Suppression of endotoxin-induced inflammation by taxol. *Eur Respir J.* (2007)
704 30:429-35. doi:10.1183/09031936.00154206
- 705 40. Zhang D, Li Y, Liu Y, Xiang X and Dong Z. Paclitaxel ameliorates
706 lipopolysaccharide-induced kidney injury by binding myeloid differentiation
707 protein-2 to block Toll-like receptor 4-mediated nuclear factor-kappaB activation
708 and cytokine production. *J Pharmacol Exp Ther.* (2013) 345:69-75.
709 doi:10.1124/jpet.112.202481
- 710 41. Yang Q, Zhang D, Li Y, Li Y and Li Y. Paclitaxel alleviated liver injury of septic
711 mice by alleviating inflammatory response via microRNA-27a/TAB3/NF-kappaB
712 signaling pathway. *Biomed Pharmacother.* (2018) 97:1424-33.
713 doi:10.1016/j.biopha.2017.11.003
- 714 42. Akhmanova A and Steinmetz MO. Control of microtubule organization and
715 dynamics: two ends in the limelight. *Nat Rev Mol Cell Biol.* (2015) 16:711-26.
716 doi:10.1038/nrm4084
- 717 43. Janke C and Bulinski JC. Post-translational regulation of the microtubule
718 cytoskeleton: mechanisms and functions. *Nat Rev Mol Cell Biol.* (2011) 12:773-86.
719 doi:10.1038/nrm3227
- 720 44. North BJ, Marshall BL, Borra MT, Denu JM and Verdin E. The human Sir2

721 ortholog, SIRT2, is an NAD⁺-dependent tubulin deacetylase. *Mol Cell.* (2003)
722 11:437-44.

723 45. Portran D, Schaedel L, Xu Z, They M and Nachury MV. Tubulin acetylation
724 protects long-lived microtubules against mechanical ageing. *Nat Cell Biol.* (2017)
725 19:391-98. doi:10.1038/ncb3481

726 46. Reed NA, Cai D, Blasius TL, Jih GT, Meyhofer E, Gaertig J, et al. Microtubule
727 acetylation promotes kinesin-1 binding and transport. *Curr Biol.* (2006)
728 16:2166-72. doi:10.1016/j.cub.2006.09.014

729 47. Balabanian L, Berger CL and Hendricks AG. Acetylated Microtubules Are
730 Preferentially Bundled Leading to Enhanced Kinesin-1 Motility. *Biophys J.* (2017)
731 113:1551-60. doi:10.1016/j.bpj.2017.08.009

732 48. Misawa T, Saitoh T, Kozaki T, Park S, Takahama M and Akira S. Resveratrol
733 inhibits the acetylated alpha-tubulin-mediated assembly of the
734 NLRP3-inflammasome. *Int Immunol.* (2015) 27:425-34.
735 doi:10.1093/intimm/dxv018

736 49. Rao S, Horwitz SB and Ringel I. Direct photoaffinity labeling of tubulin with
737 taxol. *J Natl Cancer Inst.* (1992) 84:785-8.

738 50. Khan M, Giessrigl B, Vonach C, Madlener S, Prinz S, Herbaceck I, et al.
739 Berberine and a *Berberis lycium* extract inactivate Cdc25A and induce
740 alpha-tubulin acetylation that correlate with HL-60 cell cycle inhibition and
741 apoptosis. *Mutat Res.* (2010) 683:123-30 doi:10.1016/j.mrfmmm.2009.11.001

742 51. Li CG, Yan L, Jing YY, Xu LH, Liang YD, Wei HX, et al. Berberine augments
743 ATP-induced inflammasome activation in macrophages by enhancing AMPK
744 signaling. *Oncotarget.* (2017) 8:95-109 doi:10.18632/oncotarget.13921

745 52. Alexandre J, Batteux F, Nicco C, Chereau C, Laurent A, Guillevin L, et al.
746 Accumulation of hydrogen peroxide is an early and crucial step for
747 paclitaxel-induced cancer cell death both in vitro and in vivo. *Int J Cancer.* (2006)
748 119:41-8 doi:10.1002/ijc.21685

749 53. Mackeh R, Lorin S, Ratier A, Mejdoubi-Charef N, Baillet A, Bruneel A, et al.
750 Reactive oxygen species, AMP-activated protein kinase, and the transcription

751 cofactor p300 regulate alpha-tubulin acetyltransferase-1
752 (alphaTAT-1/MEC-17)-dependent microtubule hyperacetylation during cell stress.
753 J Biol Chem. (2014) 289:11816-28 doi:10.1074/jbc.M113.507400

754 54. Liu W, Gu J, Qi J, Zeng XN, Ji J, Chen ZZ, et al. Lentinan exerts synergistic
755 apoptotic effects with paclitaxel in A549 cells via activating ROS-TXNIP-NLRP3
756 inflammasome. J Cell Mol Med. (2015) 19:1949-55 doi:10.1111/jcmm.12570

757 55. Yang LP. Oral colchicine (Colcrys): in the treatment and prophylaxis of gout.
758 Drugs. (2010) 70:1603-13. doi:10.2165/11205470-000000000-00000

759 56. Gigant B, Cormier A, Dorleans A, Ravelli RB and Knossow M.
760 Microtubule-destabilizing agents: structural and mechanistic insights from the
761 interaction of colchicine and vinblastine with tubulin. Top Curr Chem. (2009)
762 286:259-78. doi:10.1007/128_2008_11

763 57. Hise AG, Tomalka J, Ganesan S, Patel K, Hall BA, Brown GD, et al. An essential
764 role for the NLRP3 inflammasome in host defense against the human fungal
765 pathogen *Candida albicans*. Cell Host Microbe. (2009) 5:487-97.
766 doi:10.1016/j.chom.2009.05.002

767 58. Maltez VI, Tubbs AL, Cook KD, Aachoui Y, Falcone EL, Holland SM, et al.
768 Inflammasomes Coordinate Pyroptosis and Natural Killer Cell Cytotoxicity to
769 Clear Infection by a Ubiquitous Environmental Bacterium. Immunity. (2015)
770 43:987-97. doi:10.1016/j.immuni.2015.10.010

771 59. Guarda G, Braun M, Staehli F, Tardivel A, Mattmann C, Forster I, et al. Type I
772 interferon inhibits interleukin-1 production and inflammasome activation.
773 Immunity. (2011) 34:213-23. doi:10.1016/j.immuni.2011.02.006

774 60. Sato A, Ohtaki H, Tsumuraya T, Song D, Ohara K, Asano M, et al. Interleukin-1
775 participates in the classical and alternative activation of microglia/macrophages
776 after spinal cord injury. J Neuroinflammation. (2012) 9: 65.
777 doi:10.1186/1742-2094-9-65

778 61. Schenk M, Fabri M, Krutzik SR, Lee DJ, Vu DM, Sieling PA, et al.
779 Interleukin-1beta triggers the differentiation of macrophages with enhanced
780 capacity to present mycobacterial antigen to T cells. Immunology. (2014)

- 781 141:174-80. doi:10.1111/imm.12167
- 782 62. Uchiyama R, Yonehara S, Taniguchi S, Ishido S, Ishii KJ and Tsutsui H.
783 Inflammasome and Fas-Mediated IL-1beta Contributes to Th17/Th1 Cell Induction
784 in Pathogenic Bacterial Infection In Vivo. *J Immunol.* (2017) 199:1122-30.
785 doi:10.4049/jimmunol.1601373
- 786 63. Kumar H, Kumagai Y, Tsuchida T, Koenig PA, Satoh T, Guo Z, et al. Involvement
787 of the NLRP3 inflammasome in innate and humoral adaptive immune responses to
788 fungal beta-glucan. *J Immunol.* (2009) 183:8061-7.
789 doi:10.4049/jimmunol.0902477
- 790 64. Marupudi NI, Han JE, Li KW, Renard VM, Tyler BM, Brem H. Paclitaxel: a
791 review of adverse toxicities and novel delivery strategies. *Expert Opin Drug Saf.*
792 (2007) 6: 609-21. doi:10.1517/14740338.6.5.609
- 793 65. Walker FE. Paclitaxel (TAXOL): side effects and patient education issues. *Semin*
794 *Oncol Nurs.* (1993) 9: 6-10. doi:10.1016/S0749-2081(16)30036-5
795

Provisional

796 **Figure legends**

797 **Figure 1. Paclitaxel promoted NLRP3 inflammasome activation in murine**
798 **macrophages.** LPS-primed J774A.1 macrophages were pre-treated paclitaxel for 1 h
799 followed by stimulation with ATP (3 mM) for 1 h, while LPS-primed bone
800 marrow-derived macrophages (BMDMs) were pre-treated with paclitaxel for 1 h
801 followed by stimulation with ATP (2 mM) for 30 min or nigericin (5 μ M) for 1 h. (A,
802 D, G) Western blot analysis of indicated proteins in the culture supernatants and cell
803 lysates. Actin was used as a loading control. (B, C, E, F, H, I) Histograms show the
804 gray value of capase-1p10 (10 kDa) or mature IL-1 β (17 kDa) bands in supernatants
805 relative to that of ATP or nigericin group that was set to 1.0, respectively. (B, C)
806 Histograms show quantified data from the results presented in Fig. 1A. (E, F)
807 Histograms show quantified data from the results in Fig. 1D. (H, I) Histograms show
808 quantified data from the results in Fig. 1G. Data were analyzed using the
809 non-parametric Mann–Whitney U test, which are shown as mean \pm SD ($n = 3$). * $P <$
810 0.05; ** $P <$ 0.01; PTX, paclitaxel; Nig, nigericin.

811 **Figure 2. Paclitaxel increased ATP-induced ASC speck formation and pyroptosis**
812 **in bone marrow-derived macrophages (BMDMs).** LPS-primed BMDMs were
813 pre-treated with indicated concentrations of paclitaxel for 1 h, followed by incubation
814 with ATP (2 mM) for 30 min without LPS. (A) ASC expression and subcellular
815 distribution were revealed by fluorescence microscopy. Representative images (40 \times)
816 showing ASC (green) subcellular distribution. Nuclei were revealed by Hoechst
817 33342 (blue). The images for ASC and nuclei were captured under a fluorescence
818 microscope, respectively, and merged together. Yellow arrows indicate ASC specks
819 and the enlarged inset showing a cell containing an ASC speck. Scale bars, 20 μ m. (B)
820 Percentages of cells with an ASC speck relative to the total cells from 5 random fields
821 each containing \sim 50 cells. Data were analyzed using the unpaired Student's t-test,
822 which are shown as mean \pm SD ($n = 5$, one field per well). *** $P <$ 0.001. (C) Western
823 blotting was used to detect indicated proteins in cell lysates. Actin was used as the
824 loading control. (D) Histograms show the quantification of GSDMD-NT levels
825 relative to that of actin. Data were analyzed using the non-parametric Mann–Whitney
826 U test, which are shown as mean \pm SD ($n=3$). (E, F) Cell death was assayed by
827 propidium iodide (PI) (red; staining dead cells) and Hoechst 33342 staining (blue;
828 staining all cells) for 10 min. PI-positive cells in 5 randomly chosen fields (one field
829 per well) each containing \sim 100 cells were quantified (see Supplementary Figure S4A).
830 (E) The percentage of cell death is defined as the ratio of PI-positive relative to all
831 cells (revealed by Hoechst 33342). Data were analyzed using the one-way ANOVA
832 followed by Turkey post hoc test, which are shown as mean \pm SD ($n=5$). (F) Merged
833 images showing PI (red) and Hoechst 33342 (blue) fluorescence combined with
834 bright-field images. The enlarged insets show the cell morphology. One set of
835 representative images of three independent experiments is shown. Black arrows
836 indicate one dying cell with ballooning from the plasma membrane in each image.
837 Scale bars, 20 μ m. GSDMD-FL, full-length GSDMD; GSDMD-NT, GSDMD

838 N-terminal fragment; PTX, paclitaxel. ** $P < 0.01$; *** $P < 0.001$.

839 **Figure 3. Paclitaxel pretreatment increased the levels of acetylated α -tubulin.**
840 LPS-primed J774A.1 macrophages (A, B) and BMDMs (C-F) were pre-treated with
841 graded concentrations of paclitaxel for 1 h (A-D) or with paclitaxel (33 nM) for
842 indicated time periods (E, F). Western blotting was used to assess the levels of
843 indicated proteins in cell lysates (A, C, E). Actin was used as the loading control.
844 Histograms showing the quantification of acetylated α -tubulin relative to total
845 α -tubulin are shown in (B, D, F), respectively. Data were analyzed using the unpaired
846 Student's t-test (B, D) or non-parametric Mann–Whitney U test (F), which are shown
847 as mean \pm SD ($n = 3$). *** $P < 0.001$. PTX, paclitaxel.

848 **Figure 4. Resveratrol and NAD⁺ suppressed paclitaxel-mediated augmentation of**
849 **NLRP3 inflammasome activation.** (A, B) LPS-primed BMDMs were pre-treated
850 without (None) or with resveratrol (5 μ M) or NAD⁺ (10 μ M) for 30 min before
851 incubation with paclitaxel (33 nM) for 1 h and then stimulation with nigericin (5 μ M)
852 for 1 h. After staining with indicated antibodies, the cells were observed by
853 fluorescence microscopy and the images were captured, respectively, and merged
854 together. Representative immunofluorescence images showing acetylated α -tubulin
855 (red) subcellular distribution (A). Nuclei (blue) were revealed by Hoechst 33342.
856 Scale bars, 10 μ m. (B) Mean of fluorescence intensity (MFI) of acetylated α -tubulin
857 was analyzed by ZEN software. Data were analyzed using the non-parametric
858 Friedman test, which are shown as mean \pm SD ($n=5$). (C, D, E) LPS-primed BMDMs
859 were pre-treated with resveratrol (5 μ M) (C, D) or NAD⁺ (10 μ M) (E) for 30 min
860 prior to paclitaxel (100 nM) treatment for 1 h, followed by incubation with ATP (2
861 mM) for 30 min. The expression and subcellular distribution of ASC were revealed by
862 the immunofluorescent microscopy. (C) Representative images showing ASC (green)
863 subcellular distribution. Nuclei (blue) were revealed by Hoechst 33342. Yellow
864 arrows indicate ASC specks and the enlarged inset showing cells with an ASC speck.
865 Scale bars, 20 μ m. (D) Percentages of cells with an ASC speck relative to total cells
866 from 5 random fields each containing \sim 200 cells (see Supplementary Figure S5).
867 Data were analyzed using the non-parametric Mann–Whitney U test, which are shown
868 as mean \pm SD ($n = 5$). (E) Levels of soluble IL-1 β in culture supernatants were
869 analyzed by cytometric bead array (CBA) assay. Data were analyzed using the
870 one-way ANOVA followed by Turkey post hoc test, which are shown as mean \pm SD
871 ($n = 3$). * $P < 0.05$; ** $P < 0.01$; *** $P < 0.001$; PTX, paclitaxel; RSV, resveratrol.

872 **Figure 5. Paclitaxel induced α -tubulin acetylation and promoted the apposition**
873 **of ASC specks and γ -tubulin upon ATP stimulation.** LPS-primed BMDMs were
874 pretreated with resveratrol (100 nM) for 30 min and paclitaxel (100 nM) for 1 h. Then
875 the cells were stimulated with ATP (2 mM) for 30 min. Finally, indicated proteins
876 were stained by indicated antibodies and observed by immunofluorescence
877 microscopy. Bright field (BF) and immunofluorescence images were captured
878 respectively, while some of which were merged as being indicated. Enlarged insets
879 show the acetylated α -tubulin, γ -tubulin and ASC specks, as well as their subcellular

880 location. Scale bars, 10 μm .

881 **Figure 6. MEC-17 knockdown attenuated paclitaxel-mediated augmentation of**
882 **NLRP3 inflammasome activation and pyroptosis.** J774A.1 macrophages and
883 BMDMs were transfected with negative control (NC) siRNA or *MEC-17* siRNA for
884 48 h and were used for the following experiments. (A, B) The levels of MEC-17
885 expression in J774A.1 (A) or BMDMs (B) were detected by Western blotting. (C-F)
886 LPS-primed J774A.1 macrophages were treated with paclitaxel (33 nM) for 1 h. The
887 expression of acetylated α -tubulin and α -tubulin were revealed by Western blotting (C)
888 and the relative gray values of acetylated α -tubulin to α -tubulin were quantified (D).
889 Data are shown as mean \pm SD ($n = 3$). Immunofluorescence microscopy revealed the
890 expression of acetylated α -tubulin (red) and α -tubulin (green) in J774A.1 cells (E) or
891 in BMDMs (F). Nuclei were stained with Hoechst 33342 (blue). Scale bars, 10 μm .
892 (G-J) Cells were primed with LPS (500 ng/ml for 4 h) before treated with paclitaxel
893 (33 nM) for 1 h, followed by incubation with ATP (3 mM for 1 h) in J774A.1 (G, H)
894 or nigericin (5 μM for 1 h) in BMDMs (I, J). The levels of soluble IL-1 β were
895 detected by cytometric bead array (G, I). Cell death was measured by staining with
896 propidium iodide (PI) and Hoechst 33342 together for 10 min. PI-positive cells were
897 quantified by counting 5 randomly chosen fields (one field per well) containing
898 around 100 cells each (H, J). Data were analyzed using the unpaired Student's t-test,
899 which are shown as mean \pm SD ($n = 5$). * $P < 0.05$; ** $P < 0.01$; *** $P < 0.001$. PTX,
900 paclitaxel.

901 **Figure 7. Paclitaxel did not influence macrophage priming in the process of**
902 **NLRP3 inflammasome activation.** (A) BMDMs were treated with LPS (500 ng/ml),
903 paclitaxel (100 nM) and epothilone B (100 nM) for 4h. Indicated proteins in the cell
904 lysates were analyzed by Western blotting. Actin was used as a loading control. (B, C,
905 D) LPS-primed BMDMs were pre-treated with graded doses of epothilone B for 1h,
906 followed by incubation with ATP (2 mM) for 30 min. (B, C) Cells were stained by
907 Hoechst 33342 (blue; for all cells) and propidium iodide (PI) (red; for dead cells) for
908 10 min. (B) All images were captured by fluorescence microscopy, and the merged
909 images show PI and Hoechst 33342 fluorescence with bright-field images. One set of
910 representative images of three independent experiments are shown. Scale bars, 50 μm .
911 (C) PI-positive cells in 5 randomly chosen fields (one field per well) each containing
912 \sim 100 cells were quantified. The percentage of cell death is defined as the ratio of
913 PI-positive relative to all (revealed by Hoechst 33342) cells. (D) The levels of soluble
914 IL-1 β in culture supernatants were analyzed by cytometric bead array (CBA) assay.
915 (C, D) Data were analyzed using the one-way ANOVA followed by Turkey post hoc
916 test, which are shown as mean \pm SD ($n = 5$). * $P < 0.05$; ** $P < 0.01$; *** $P < 0.001$;
917 PTX, paclitaxel; EpoB, Epothilone B.

918 **Figure 8. Paclitaxel administration prolonged mouse survival during bacterial infection.**
919 (A) Mice were injected (i.p.) with paclitaxel (5 and 10 mg/kg body weight) or vehicle (PBS) 1
920 h before peritoneal injection with viable *Escherichia coli* (2×10^9 CFU/mouse). Mouse
921 survival was monitored every 6 h for five consecutive days. Kaplan–Meier survival curves

922 were used to analyze the data (10 mice per group). The significance was evaluated by the
923 log-rank (Mantel–Cox) test. Three independent experiments were performed and one
924 representative set of data were shown. $**P < 0.01$; $***P < 0.001$. **(B, C, D)** Mice were
925 injection (i.p.) with paclitaxel (10 mg/kg body weight) or vehicle (PBS) 1 h before peritoneal
926 injection with viable *E. coli* (1×10^9 CFU/mouse) for 8 h. Bacterial counts in the peritoneal
927 cavity was measured by using an ultraviolet-visible spectrophotometer, and the
928 corresponding CFUs were determined on LB media agar plates **(B)**. The serum levels
929 of IL-1 β were measured by cytometric bead array (five mice per group) **(C)**. **(B, C)**,
930 Data were analyzed using the unpaired Student's t-test, which are shown as mean \pm
931 SD ($n = 5$). $*P < 0.05$; $***P < 0.001$. Representative images of hematoxylin and eosin
932 (H&E) staining of the liver section are shown and arrowheads indicated infiltrated
933 inflammatory cells **(D)**. The numbers at the bottom indicate mouse number. Scale bars, 100
934 μm . PTX, paclitaxel.

935

Provisional

Figure 01.TIF

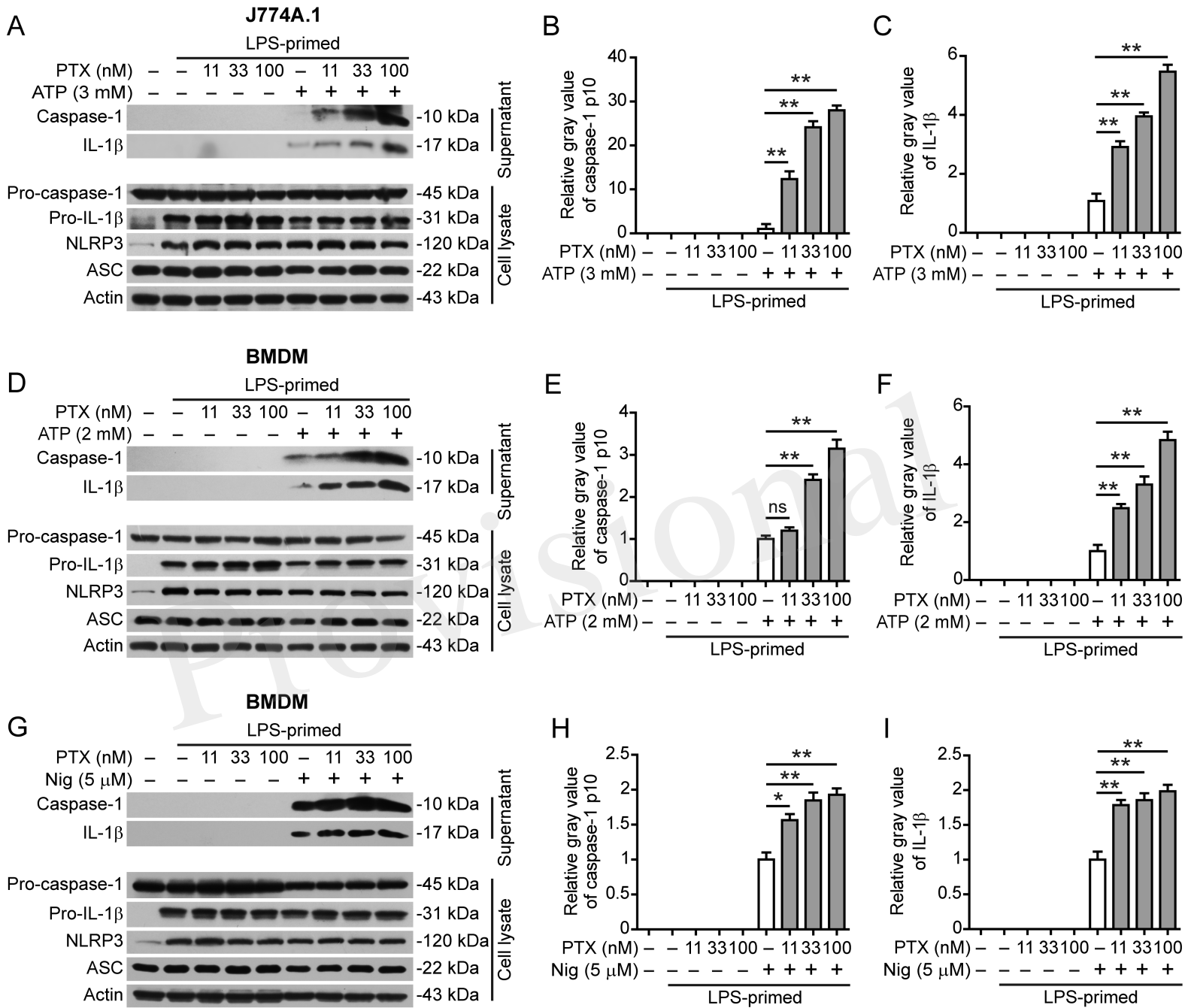
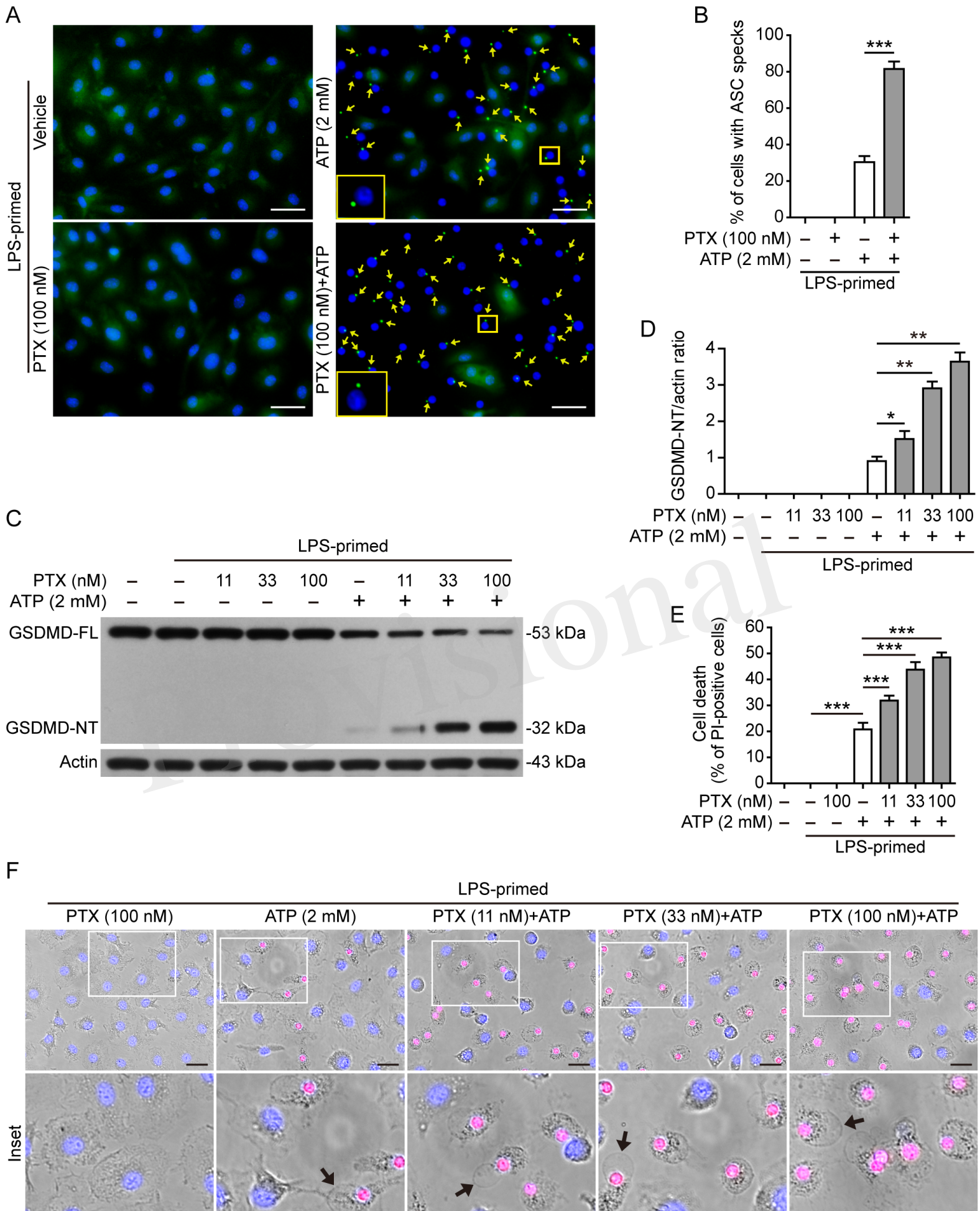


Figure 02.TIF



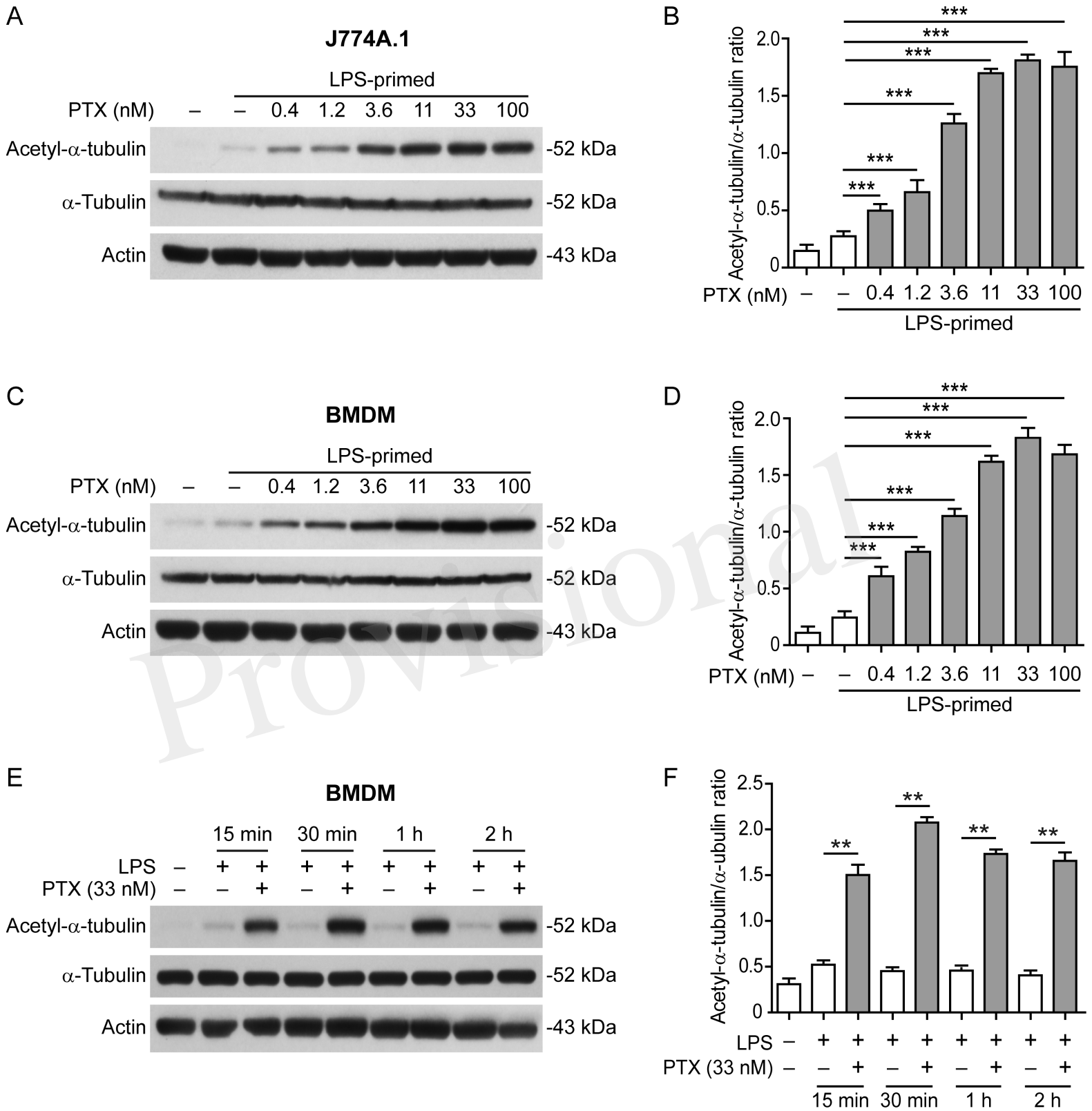


Figure 04.TIF

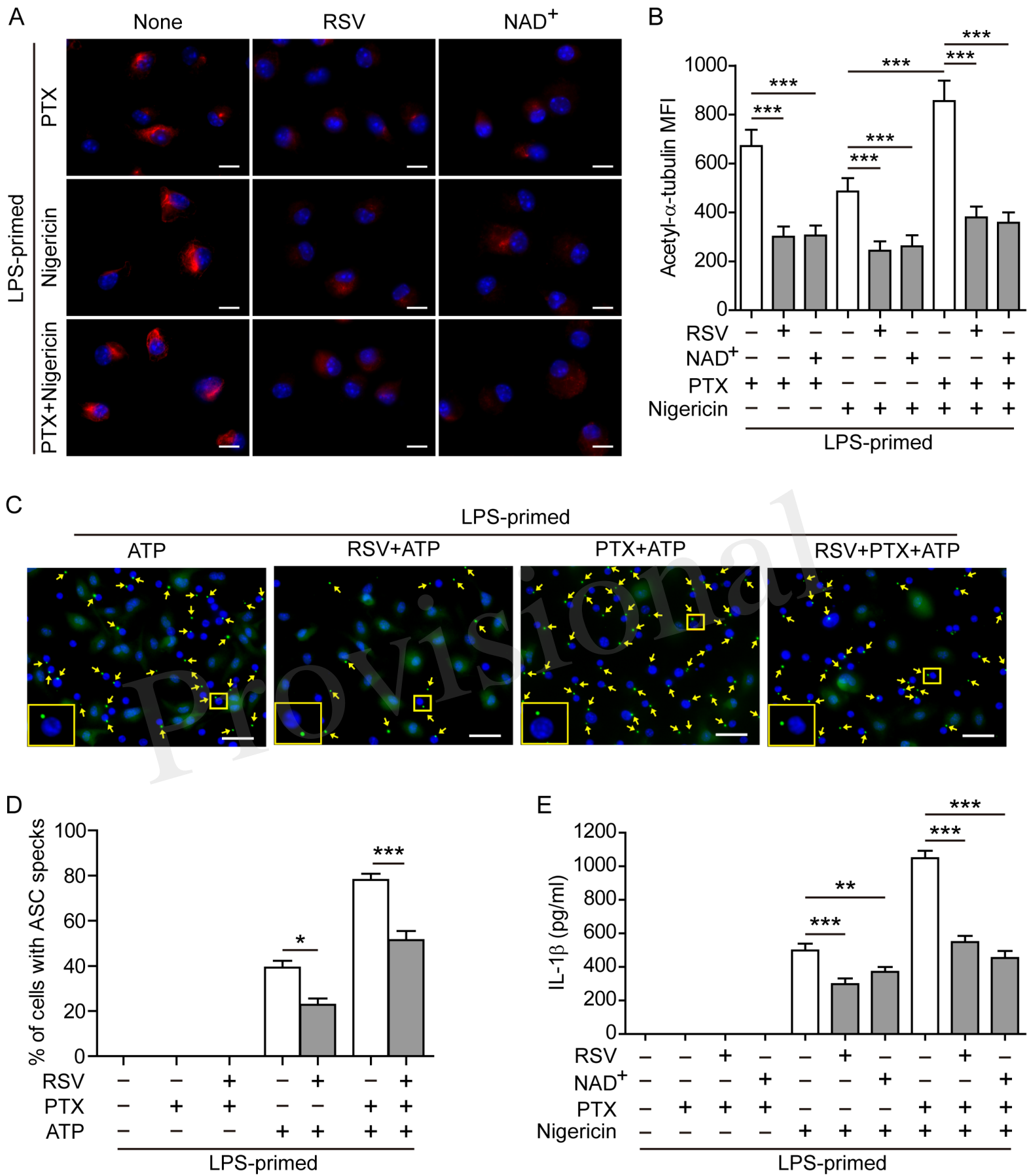


Figure 05.TIF

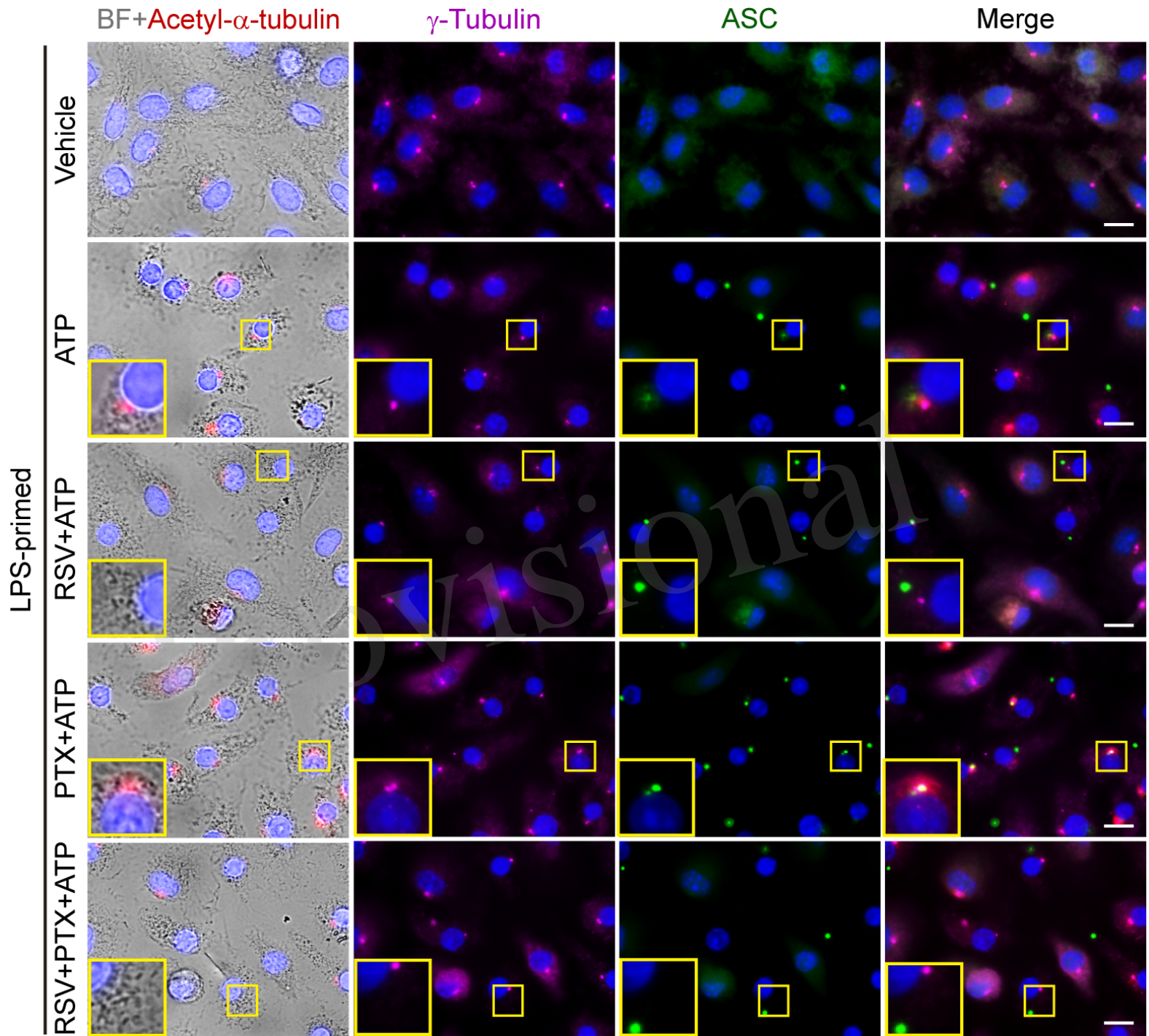


Figure 06.TIF

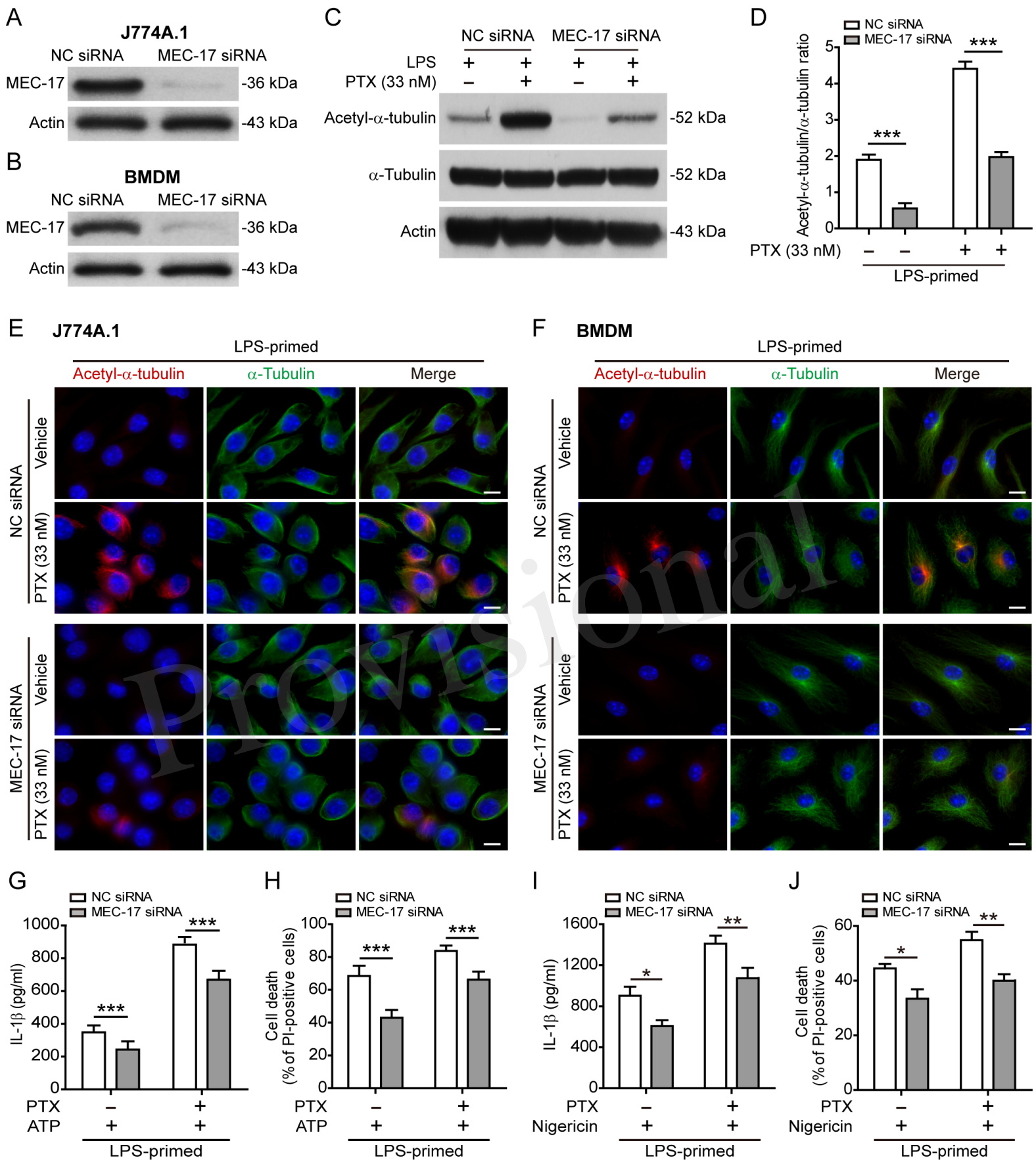


Figure 07.TIF

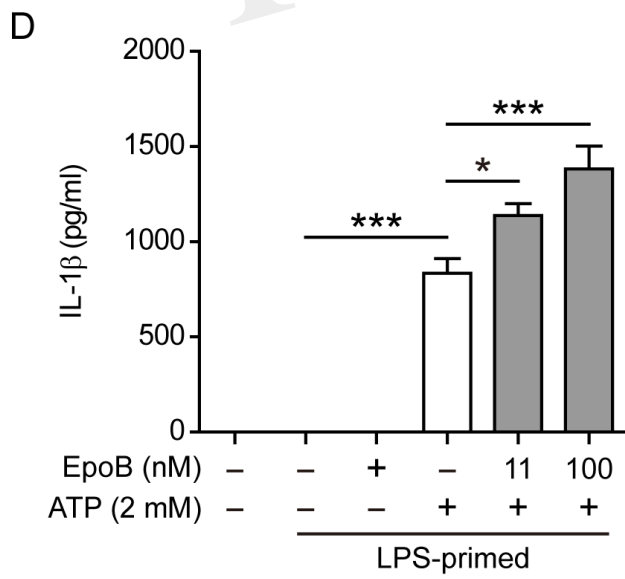
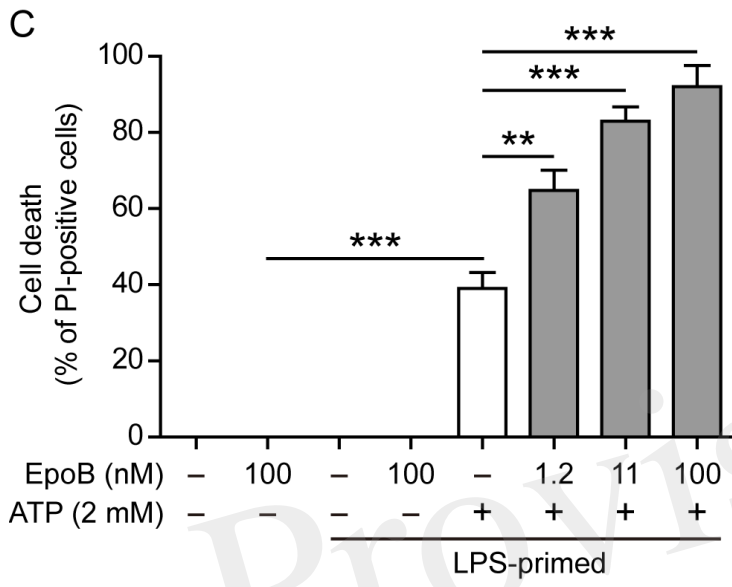
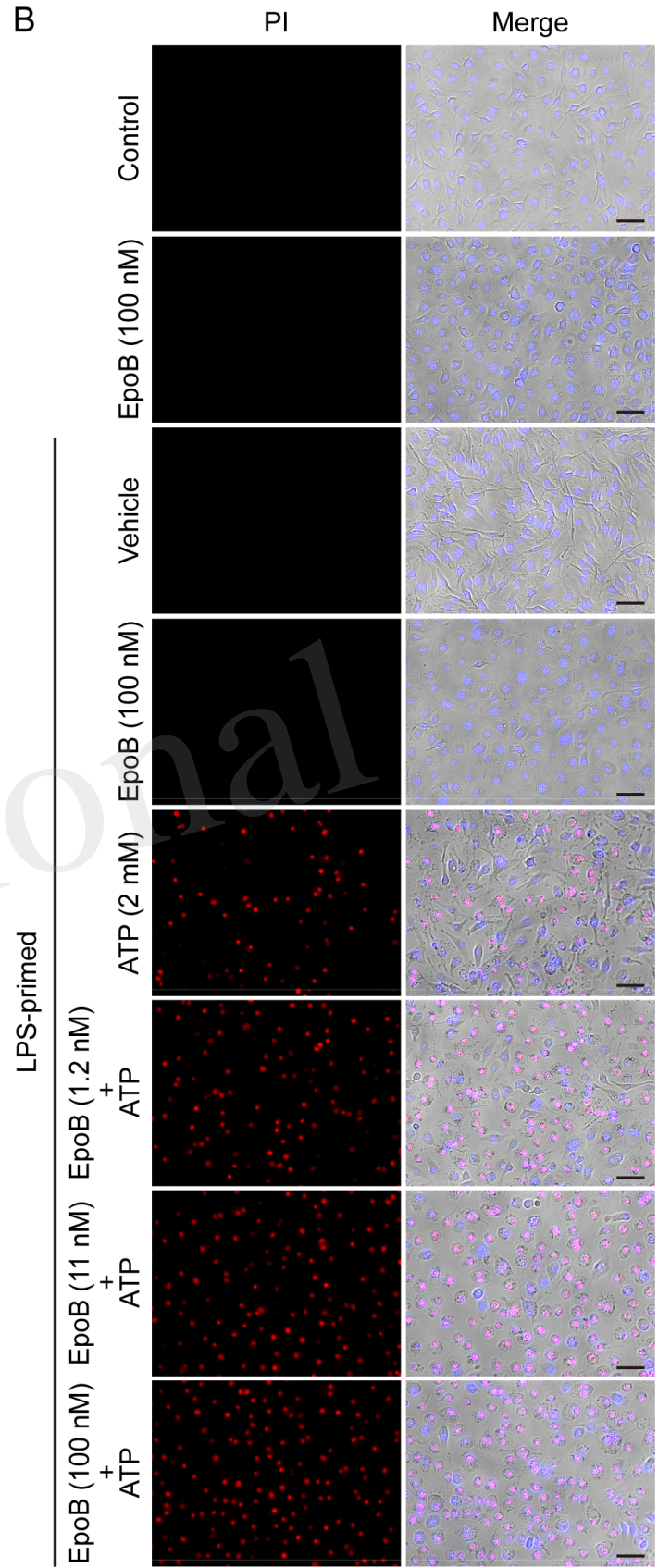
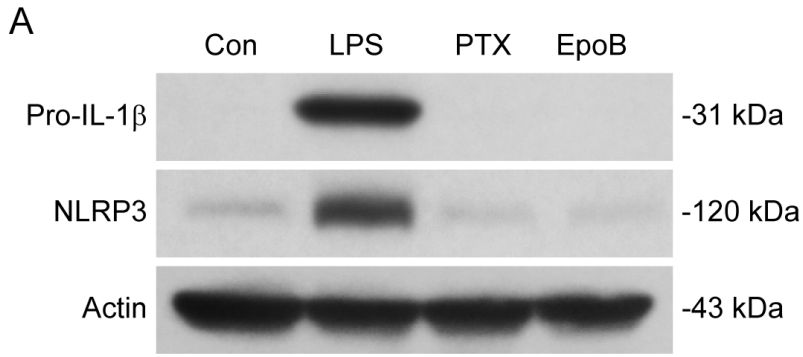


Figure 08.TIF

